Stimulation of phospholipase Cβ1 by $G\alpha_q$ promotes the assembly of stress granule proteins

Androniqi Qifti[1*], Lela Jackson[1*], Ashima Singla[1‡], Osama Garwain[1§], Suzanne Scarlata[1†]

[1]Department of Chemistry and Biochemistry, Worcester Polytechnic Institute, Worcester, MA 01609, USA.

[*]These authors contributed equally to this study.

[‡]Current address: SCO 2A Madhya Marg, Sector 7-C, Chandigarh, 160007 India.

[§]Current address: Agilent Technologies, Santa Clara, CA 95051

[†]Corresponding author. Email: sfscarlata@wpi.edu

ABSTRACT

During adverse conditions, mammalian cells regulate protein production by sequestering the translational machinery in membrane-less organelles known as stress granules. Here, we found that activation of the G protein subunit $G\alpha_q$ promoted the formation of particles that contained stress granule proteins through a mechanism linked to the presence of phospholipase Cβ1 (PLCβ1) in the cytosol. In experiments with PC12 and A10 cells, we showed that under basal conditions, cytosolic PLCβ1 bound to stress granule-associated proteins, including PABPC1, eIF5A, and Ago2. Knockdown of cytosolic PLCβ1 with siRNA or promoting its relocalization to the plasma membrane by activating $G\alpha_q$ resulted in the formation of particles containing the stress granule markers, PABPC1, G3BP1, and Ago2. Our studies showed that the composition of these particles resemble those formed under osmotic stress and are distinct from those formed by other stresses. Our results fit a simple thermodynamic model in which cytosolic PLCβ1 solubilizes stress granule proteins such that its movement to activated $G\alpha_q$ releases these particles to enable the formation of stress granules. Together, our data are suggestive of a link between $G\alpha_q$-coupled signals and protein translation through stress granule formation.

INTRODUCTION

When cells are subjected to environmental stresses, they halt the production of many housekeeping proteins to preserve resources for the synthesis of proteins that will help the cell alleviate the particular stress. These stalled translation complexes, called stress granules, are thought to act as triage sites that protect nontranslated mRNAs from degradation until the stress is removed, while enabling the synthesis of other proteins (*1, 2*). Stress granules are distinct from processing bodies (P-bodies) that store and process mRNA, although these have also been observed under nonstress conditions. Depending on the cellular conditions, the mRNA held in these stalled complexes may be degraded, translated, or stored until needed. Additionally, studies in yeast subjected to hypo-osmotic stress found that P-bodies and stress granules may form hybrid structures (*3*), although this behavior has not yet been observed in higher eukaryotes. Physically, stress granules are phase-separated domains composed of nontranslating mRNAs, translation initiation complexes, poly (A)–binding protein, and many additional mRNA-related proteins (*4*). They consist of a packed core with loosely associated peripheral proteins (*5*). Stress granules appear when cells are subjected to environmental conditions such as cold- or heat-shock, exposure to toxic molecules, oxidative stress, hypo- or hyper-osmolarity, UV irradiation, or nutrient deprivation. The molecular mechanisms that transduce these different stresses into the cellular interior remain largely unresolved. Although stress granules appear in many types of cells, we focused here on those that form in mammalian cells. Stress granules have been implicated in the pathogenesis of various diseases, such as cancer, neurodegeneration, and viral infections (*1, 6*). Many stress granule proteins contain disordered regions, which play important roles in the liquid-like nature of stress granules. Neuronal cells, in particular, contain many proteins with disordered regions, and so it is

not surprising that some neurological diseases (for example, amyotrophic lateral sclerosis) have been attributed to the abnormal stability of stress granules (*7*). Thus, it is important that cells have mechanisms to prevent the premature formation of stress granules, as well as to ensure their reversible assembly and disassembly.

Whereas stress granules primarily contain proteins associated with translation, note that argonaute 2 (Ago2) can be found in these regions (*8*). Ago2 is the main nuclease component of the RNA-induced silencing complex (RISC) (*9*). Ago2 binds to small interfering RNAs (siRNAs) in their double-stranded form and holds the guide strand after the passenger strand is degraded to enable hybridization with a target mRNA. If pairing between the passenger strand and the mRNA is perfect, as is the case with exogenous siRNAs, then Ago2 will undergo conformational changes that result in mRNA degradation. Alternatively, if pairing is imperfect, as is frequently the case for endogenous microRNAs (miRNAs), the conformational changes that enable Ago2 nuclease activity do not occur, which results in the formation of a stalled complex (*10*). Thus, the formation and stability of these stalled complexes and their incorporation into stress granules alter protein populations, which may modify downstream protein-protein interactions that may ultimately change the properties of the cell.

The mechanisms through which environmental changes are transduced into the cell to promote stress granule formation are unclear and are likely to differ with different types of stress. Here, we showed that extracellular signals can affect stress granule formation through heterotrimeric guanine nucleotide–binding proteins (G proteins) to stall protein translation. Signaling through G proteins is initiated when external ligands bind to their target G protein–coupled receptors

(GPCRs), which activates intracellular Gα subunits. The $G\alpha_q$ family of G proteins is activated by GPCRs for agents such as acetylcholine, dopamine, bradykinin, serotonin, and histamine (*11, 12*). Activated $G\alpha_q$ in turn activates phospholipase Cβ (PLCβ), which catalyzes the hydrolysis of the signaling lipid phosphatidylinositol-4, 5-bisphosphate, which eventually results in an increase in intracellular calcium (Ca^{2+}) signaling. There are four known members of the PLCβ family differ in their tissue distribution and their ability to be activated by G proteins (*12*). Here, we focused on PLCβ1, which is the isoform most highly activated by $G\alpha_q$ and is prominent in neuronal tissue. Whereas the major population of PLCβ1 lies at the plasma membrane, where it binds to $G\alpha_q$ and accesses its substrate, PLCβ1 is also found in the cytosol in every cell type examined and under different conditions (*13, 14*).

We previously found that cytosolic PLCβ1 binds to C3PO, the promoter of RNA-induced silencing, and showed that this binding can reverse the RNA-induced silencing of specific genes (*14, 15*). The association between these two proteins occurs in the same region through which $G\alpha_q$ binds to PLCβ1 and is upstream of the active site. Thus, although the catalytic activity of PLCβ1 is not affected by the binding of C3PO, its ability to be activated by $G\alpha_q$ is eliminated. Subsequent studies showed that the association between PLCβ1 and C3PO is critical for PC12 cell differentiation (*16, 17*); however, little or no association is seen in nondifferentiating cells, leading to the question of whether cytosolic PLCβ1 has other binding partners. We also found that PLCβ1 binds to and inhibits a neuronal-specific enzyme required for cellular proliferation, CDK16 (*18, 19*), and that this association enables cells to cease proliferation and transition into a differentiated state (*17*). Again, this association is confined to a specific event that drives neuronal cells out of stemness, and suggests that under nonproliferating, nondifferentiating conditions, cytosolic PLCβ1

serves some other function. Here, we showed that a major population of cytosolic PLCβ1 was bound to stress granule–associated proteins and that this binding prevented premature stress granule formation. Removal of PLCβ1 from the cytoplasm in response to stress or by $G\alpha_q$-mediated stimulation promoted stress particle assembly. The interaction between PLCβ1 and stress granule proteins suggests a previously uncharacterized feedback mechanism between the external environment and the protein translation machinery.

RESULTS

PLCβ1 binds to stress granule–associated proteins

We began this work by performing experiments to determine previously uncharacterized binding partners of cytosolic PLCβ1 in PC12 cells under nondifferentiating conditions. Our approach was to isolate the cytosolic fractions of unsynchronized, undifferentiated PC12 cells and use a monoclonal antibody to pull down proteins bound to PLCβ1. We collected the PLCβ1-bound proteins and identified them by mass spectrometry (MS) analysis. Unexpectedly, we found that ~30% of the total proteins associated with cytosolic PLCβ1 were markers for stress granules (table S1) (*1, 20*), and we determined the percentage of their contribution to the total intensity (Fig. 1A). In contrast, control studies with cytosolic fractions of cells with reduced amounts of PLCβ1 identified nonspecific proteins, such as tubulin, actin, and mitochondrial proteins (table S2).

These studies (Fig. 1A) were performed with unsynchronized cells where ~90% were in the G1 phase (*17*). However, our previous studies suggested that PLCβ1 may change binding partners as cells move through the cell cycle (*21*). Additionally, PLCβ1 has a nuclear population that may exchange with the cytosolic one (*22*). Therefore, we repeated the studies in cells in which the

nuclear population of PLCβ1 was also available for binding by arresting cells in the G2/M phase, during which the nuclear matrix has broken down (Fig. 1B and table S3). Again, we found that 32% of the proteins bound to PLCβ1 were markers for stress granules, with the most prominent being eukaryotic initiation factor 5A (eIF5A) and polyadenylate binding protein C1 (PABPC1) (Fig. 1B). Additionally, other stress granule and translation proteins appeared in both groups, including FXR1/2, G3BP1, and other eIF proteins. Note that Ago2, which is associated with both RISCs and stress granules (*8*), appeared in these cells.

The proteomics studies described earlier are only indicative of potential protein partners of PLCβ1, because the candidates were identified under nonphysiological conditions. Therefore, we verified the binding of PLCβ1 to stress granule proteins through several other methods. First, we again performed pull-down experiments with the same monoclonal antibody that we used earlier, and we detected the association of two stress granule proteins by Western blotting analysis. The first, PABPC1, is an established marker for stress granules (*20*). The second, Ago2, moves into granules under stress conditions (*8*). Using unsynchronized, undifferentiated PC12 cells, we verified that PABPC1 and Ago2 bound to PLCβ1 (Fig. 1, C and D). We then determined whether the amounts of these proteins changed when two of the established binding partners of PLCβ1, $G\alpha_q$ and C3PO, were over-expressed (Fig. 1C, fig. S1, A and B, and fig. S2 A and B). We found that the amount of Ago2 that bound to PLCβ1 was reduced when that of either of the binding partners was increased, suggesting that Ago2 bound to similar regions of PLCβ1. However, the amount of PABPC1 that was pulled down with PLCβ1 did not significantly change with over-expression of either $G\alpha_q$ or C3PO ($P = 0.81$ and $P = 0.54$, respectively) and was reduced when Ago2 was over-expressed. The simplest interpretation of these data is that the interaction between PLCβ1 and

PABPC1 differs from that between PLCβ1 and Ago2, and that the reduction in PABPC1 abundance in cells overexpressing Ago2 may be due to a redistribution of the PLCβ1 pool.

We wanted to verify that similar results could be obtained from experiments in which a different PLCβ1 antibody was used. Noting that PLCβ1 differs from other PLCβ family members mainly in the long 400 amino acid C-terminal domain to which $G\alpha_q$ and C3PO bind, and where some stress granule proteins may bind, we repeated the pull-down experiments under conditions in which antibody binding to its epitope in PLCβ1 would not occlude any potential binding partners. Specifically, we transfected undifferentiated, unsynchronized PC12 cells with a plasmid expressing eGFP-PLCβ1 where the eGFP tag is tethered to the N terminus of PLCβ1 and performed the pull-down experiments with anti-eGFP antibody. The results (Fig. 1C and D and fig. S3) showed associations between PLCβ1 and PABPC1, Ago2, and G3BP1. Together, these data support the idea that cytosolic PLCβ1 interacts with stress granule-associated proteins.

PLCβ1 associates with Ago2 but not G3BP1 in live cells

Our earlier studies suggested that the interaction between PLCβ1 and Ago2 might be modulated by G protein stimulation and cellular events associated with C3PO. Keeping in mind that C3PO promotes RNA-induced silencing, we set out to characterize the factors that regulated the PLCβ1-Ago2 association. We first isolated the cytosolic fractions of unsynchronized, undifferentiated PC12 cells, pulled down proteins associated with Ago2, and identified them by MS. We found that PLCβ1 was included in the data set (table S4). Note that all of the proteins that were associated with PLCβ1 (Fig. 1A) were also pulled down with Ago2 (table S4).

We measured the extent of the association between PLCβ1 and Ago2 in live PC12 cells by Förster resonance energy transfer (FRET) as monitored by fluorescence lifetime imaging microscopy (FLIM). In this method, FRET efficiency is determined by the reduction in the time that the donor spends in the excited state, or the fluorescence lifetime, before transferring energy to an acceptor fluorophore (*23*). If the donor molecule is excited with light that has a modulated intensity, the lifetime can be determined by the reduction in modulated intensity (M) as well as the shift in phase (φ) of the emitted light. If FRET occurs when the donor is in the excited state, the fluorescence lifetime will be reduced as indicated by a reduced change in modulation and phase shift. The amount of FRET can then be directly determined from the raw data by plotting the lifetimes in each pixel in the image on a phasor plot [S versus G, where S = M*sin (φ) and G = M*cos (φ)] (*24*). In these plots, the lifetimes in each pixel in a FLIM image will fall on the phasor arc for a single population. However, when two or more lifetimes are present, the points will be a linear combination of the fractions, with the points inside the phase arc that move towards the right due to shortened lifetimes such as when FRET occurs. Note that phasor representation is simply the Fourier transform of the lifetime decay curves but readily displays lifetimes directly from raw data without the need for model-dependent fitting of the lifetimes or other corrections.

Thus, we generated the phasor plot and the corresponding image of a PC12 cell expressing eGFP-PLCβ1 presenting the phase and modulation lifetime of each pixel in the image (Fig. 2, A to C). As expected for a single lifetime species, all points fell on the phasor arc (Fig. 2A). When we repeated this experiment with cells expressing both eGFP-PLCβ1 and mCherry-Ago2, where mCherry is a FRET acceptor, the average donor lifetime was reduced from 2.5 to 1.7 ns and the points moved inside the phasor (Fig. 2B). This reduction in lifetime and movement of the points

into the phasor showed the occurrence of FRET between the probes. Because the amount of FRET depends on the distance between the fluorophores to the sixth power and given that the distance at which 50% transfers for the eGFP-mCherry pair is ~30 Å (*25*), our results suggest a direct interaction between PLCβ1 and Ago2 in the cytosol. We could select points in the phasor plots and visualize their localization in the cell image. We found that the points corresponding to FRET, and thus eGFP-PLCβ1:mCherry-Ago2 complexes, were localized in the cytoplasm (Fig. 2C). In contrast, points corresponding to eGFP-PLCβ1 alone were found both on the plasma membrane and in the cytoplasm. Additionally, we tested the extent of the association between eGFP-PLCβ1 and eGFP-G3BP1 using homo-FRET or FRET between identical species. No changes in lifetime, and thus no FRET, were detected (fig. S2). This absence of FRET indicates that the two fluorophores were separated by more than ~45 Å, which suggests that any association between the two proteins is indirect.

eIF5A binds to PLCβ1 competitively with C3PO and $G\alpha_q$

To remain cytosolic, stress granule proteins would need to bind to PLCβ1 in a manner competitive with $G\alpha_q$ or it would localize to the plasma membrane. We previously showed that PLCβ1 binds to C3PO through the same C-terminal region with which it binds to $G\alpha_q$ (*15*), and that competition between C3PO and $G\alpha_q$ regulates the ability of PLCβ1 to generate Ca^{2+} signals through $G\alpha_q$ activation or the ability of siRNAs to promote silencing, respectively (*26*). With this in mind, we searched the proteins identified in our MS analysis for stress granule proteins that could sequester PLCβ1 from $G\alpha_q$. We noted that eIF5A, which is a GTP-activating protein (*27*), has homologous regions to the GTPase region of $G\alpha_q$ and appeared in our MS screen as a PLCβ1-binding protein, so we chose it for further testing.

In an initial study, we purified PLCβ1 and covalently labeled it with a FRET donor, Alexa Fluor 488. We then purified eIF5A, labeled it with the FRET acceptor Alexa Fluor 594, and measured the association between the two proteins in solution by fluorescence titrations similarly to previous studies (*28*). We found that the two proteins bound to each other with strong affinity ($K_d = 27 \pm 5$ nM). However, when we formed the Alexa488-PLCβ1-C3PO complex and titrated Alexa594-eIF5A into the solution, we could not detect FRET (fig. S4). This result suggests that eIF5A binds to the same region of PLCβ1 as does C3PO, and similarly, to $G\alpha_q$ (*15*). To determine whether eIF5A competed with C3PO for binding to PLCβ1 in cells, we transfected PC12 cells with plasmids expressing eGFP-PLCβ1 and mCherry-TRAX to produce fluorescent C3PO (*29*). We detected an association between the two proteins by FLIM/FRET measurements (Fig. 2, D and E). We then microinjected purified eIF5A into the cells to increase its intracellular concentration by ~10 nM and found that FRET was eliminated (Fig. 2F). This result suggests that eIF5A displaces C3PO from PLCβ1 and that both proteins bind to a similar region of PLCβ1 (Fig. 2G).

We confirmed our hypothesis that eIF5A binds to the C-terminal region of PLCβ1 in experiments with purified proteins in solution. In these studies, we formed the eIF5A-PLCβ1 complex, chemically cross-linked the proteins, digested the samples, separated the fragments by electrophoresis, and sequenced the peptides by MS (fig. S5, table S5). We found several interaction sites between the two proteins, but one of the most prominent was between residues 1085 to 1095 of PLCβ1and residues 97 to 103 of eIF5A (table S5), which are expected to be close to the $G\alpha_q$ activation region. Together, these studies suggest that eIF5A competes with both $G\alpha_q$ and C3PO for binding to PLCβ1 and thus could direct PLCβ1 to complexes containing stress granule proteins.

Osmotic stress has different effects on PLCβ1 isoforms

To determine whether PLCβ1 could affect stress granule formation, we subjected cells to mild, hypo-osmotic stress (300 to 150 mOsm), which we previously showed has reversible effects on the $G\alpha_q$-PLCβ signaling pathway in muscle cells as seen in figure 3(A-E) (*30, 31*). We first determined whether hypo-osmotic stress affected the association between PLCβ1 and stress granule proteins within 5 min before adaptive changes in the cell occurred.

Of the two major subtypes of PLCβ1 (1a and 1b), the 1a form is the best characterized and most prevalent subtype, having additional residues in its C terminus (residues 1142 to 1216) compared to the 1b isoform (*32*). Although both isoforms are similarly activated by $G\alpha_q$, some studies showed differences in their localization, although these differences appear to be cell type–specific (*33-35*). We found that 5 min of exposure of PC12 cells to osmotic stress caused a marked reduction in PLCβ1a abundance, whereas the amount of PLCβ1b was relatively unchanged (Fig. 3A). $G\alpha_q$ stimulation by the addition of carbachol did not affect the abundance of either isoform. Tracking the total amount of PLCβ1 with an antibody that recognizes both isoforms, we found that the cytosolic fraction of PLCβ1 was preferentially reduced by osmotic stress (Fig. 3B). Considering that the half-life of total PLCβ1 in PC12 cells is 20 min (*17*), our findings (Fig. 3, A and B) suggest that osmotic stress enhances PLCβ1a degradation. After 30 min of stress, the abundance of PLCβ1b increased compared to that in control cells, as did the amount of PABPC1, but PLCβ1a abundance remained low as the cells adapted (Fig. 3B). Because we could not distinguish between the 1a and 1b isoforms of PLCβ1 in most of our experiments, we will refer only to PLCβ1.

We determined the ability of hypo-osmotic stress to affect Ca^{2+} signals generated by $G\alpha_q$ in response to 1 μM carbachol. Using the fluorescent calcium indicator, Calcium Green (see Materials and Methods), we first verified that reducing the osmolarity from 300 to 150 mOsm did not affect the intracellular Ca^{2+} concentration. However, osmotic stress quenched the increase in Ca^{2+} signaling in response to activation of the $G\alpha_q$-PLCβ1 pathway (Fig. 3C). This loss was consistent with the reduced PLCβ1 abundance in cells under hypo-osmotic stress.

The abundance of cytosolic PLCβ1 affects stress granule assembly

It is possible that PLCβ1 binds to stress granule–associated proteins to prevent the premature assembly of stress particles. To test this idea, we followed stress granule formation in PC12 cells under hypo-osmotic stress by counting the number of particles that formed in undifferentiated, unsynchronized PC12 cells using a 100x objective lens under normal (300 mOsm) and hypo-osmotic (150 mOsm) conditions. Note that at this resolution, we may not have captured the formation of small particles (*5*), and we might have observed the assembly of primary particles, as well as the fusion of small pre-formed ones. In our experiments, we analyzed particle numbers and sizes in 1.0-μm slices though several cells and reported particle sizes in area as seen for each slice. Note also that converting the particles into three dimensions and analyzing the particles gave identical results but with reduced resolution.

We fixed PC12 cells under normal and hypo-osmotic conditions and stained them with monoclonal antibodies against the stress granule marker, PABPC1. In this analysis, we measured the size and number of particles in each slice of a confocal volume (see Materials and Methods) and plotted

the additive values of these data. Thus, the highest value plotted (Fig. 4) corresponds to the total area of the cell occupied by stress granule particles. In control cells, PABPC1 antibody staining showed ~750 particles that were less than 25 μm^2 in area (Fig. 4A). When PLCβ1 abundance was reduced by siRNA, we observed an increase in PABPC1 particle size from 25 to 100 μm^2, suggesting that the loss of PLCβ1 promoted the formation of larger particles. When we applied osmotic stress to the cells, we observed an increase in the number of PABC1-containing particles between 25 and 50 μm^2 in area (Fig. 4B) However, osmotic stress did not change the size or number of PABC1-containing particles in cells in which PLCβ1a had been reduced, suggesting that osmotic stress and the loss of PLCβ1 were not additive effects. In another series of experiments, we stimulated cells with carbachol to activate $G\alpha_q$ (Fig. 4C). We found that such stimulation induced the formation of a high number of particles of up to ~150 μm^2 in area and that reducing PLCβ1 abundance did not substantially affect either the size or number of PABPC1-containing particles. Together, these findings suggest that depletion of cytosolic PLCβ1, through siRNA treatment, osmotic stress, or recruitment to activated $G\alpha_q$, promoted the incorporation of PABPC1 into larger aggregates. We then used immunofluorescence analysis to test the effect of PLCβ1 on the size and number of particles associated with Ago2. For Ago2, the number of smaller particles substantially increased when PLCβ1 abundance was reduced (Fig. 4D). Unlike PABPC1-associated particles, the size and number of Ago2-associated particles were not affected by osmotic stress, although an increase in the number of small particles was still seen when PLCβ1 abundance was reduced (Fig. 4E). Additionally, carbachol-dependent stimulation of $G\alpha_q$ resulted in an increase in the number of Ago2-containing small particles (Fig. 4F).

The experiments described earlier were performed with fixed, stained cells. We also followed particle formation in live PC12 cells transfected with plasmids expressing mCherry-Ago2 or eGFP-G3BP1. Although the number and areas of the particles varied somewhat with the extent of transfection, the results showed the same trend as those from the immunostained samples (fig. S6, A and B), that $G\alpha_q$ stimulation or osmotic stress increased the number of Ago2-associated smaller particles. These studies suggest that reduction of cellular PLCβ1 abundance increases the number of particles of proteins associated with stress granules. Whereas the increase in particle assemblies could be due to the loss of cellular PLCβ1, it may also be due to the removal of PLCβ1 from pre-formed particles. To address this question, we transfected PC12 cells with plasmid expressing eGFP-PLCβ1 and analyzed their particles (fig. S6C). We could not detect many particles less than 400 μm^2 in area, beyond which, the number the number of particles increased to ~1000. No substantial differences were found in cells subjected to osmotic stress. These data suggest that PLCβ1 does not associate with large particles in the cell.

The differences in the size and number of PABPC1- versus Ago2- or G3BP1-containing particles suggest that they might partition into different types of granules. We tested this idea by monitoring the effect of both PLCβ1 and osmotic stress on the colocalization between Ago2 and PABPC1 (Fig. 3, D and E). Under normal osmolarity, we found little colocalization between the proteins in cells either with endogenous amounts of PLCβ1 or in cells in which PLCβ1 was knocked down. However, when the cells were subjected to osmotic stress, colocalization between Ago2 and PABPC1 increased, and this increase was greater in cells in which PLCβ1 was knocked down. These results suggest that PABPC1 and Ago2 form distinct particles that may begin to fuse or associate under high stress conditions, such as loss of cytosolic PLCβ1 or osmotic stress.

Assembly of Ago2- and G3BP1-containing aggregates depends on the type of environmental stress

It is probable that osmotic stress produces granules that are different in size, number, and composition than those produced by other stresses. We compared the formation of Ago2- and G3BP1-containing particles under different types of stress by Number & Brightness (N&B) analysis (see Materials and Methods). This method measures the number of fluorescent molecules associated with a diffusing particle in live cells (*36*). Thus, N&B measurements of cells expressing eGFP-Ago2 would indicate the conditions that promote the formation of aggregates.

We followed Ago2 aggregation in PC12 cells subjected to various stress conditions (Fig. 5 A to C). Subjecting cells to osmotic stress shifted the distribution of eGFP-Ago2 particles to the point where ~60% of the eGFP-Ago2 were significantly larger than monomers (Fig. 5B). Note that these Ago2-containing particles formed throughout the cytoplasm, and that only 75 to 80% of the cells showed aggregation. We compared the aggregation of eGFP-Ago2 in cells subjected to other stresses: cold shock (12^{o}C for 1 hour), heat shock (40^{o}C for 1 hour), treatment with 0.5 mM arsenite for 10 min (fig. S8 A to C), and oxidative stress (1 mM $CoCl_2$ for 8 hours; fig. S8D). Unlike osmotic stress, these other stresses produced changes in all of the cells observed; however, eGFP-Ago2 aggregates were seen as a few large particles rather than being evenly distributed through the cell. In a final series of experiments, we stimulated cells under normal conditions with carbachol to activate $G\alpha_q$ and promote the relocalization of cytosolic PLCβ1 to the plasma membrane (Fig. 5C). Unlike for the other stresses, we observed the formation of small eGFP-Ago2 aggregates distributed throughout the cytosol. This behavior was seen in every cell tested. These

data suggest that different stresses, including $G\alpha_q$ activation, result in patterns of formation of particles containing multiple Ago2 molecules. We also viewed the aggregation of eGFP-G3BP1 expressed in undifferentiated, unsynchronized PC12 cells (Fig. 5D to G). Unlike cells expressing eGFP-Ago2, PC12 cells expressing eGFP-G3BP1 showed aggregation under untreated conditions, (Fig. 5D), and the extent of this aggregation increased with hypo-osmotic stress (Fig. 5E), treatment with PLCβ1-specific siRNA, (5F), and carbachol treatment (Fig. 5G). Unlike the punctate pattern seen for eGFP-Ago2, eGFP-G3BP1 aggregates were more diffuse and occurred close to the plasma membrane, suggesting that eGFP-G3BP1 was present in a range of different stress granules.

Cytosolic PLCβ1 abundance affects the size of cytosolic RNAs

The formation of stress granules is expected to be accompanied by an increase in the size distribution of cytosolic RNA as mRNA accumulates due to the arrest of translation. We measured the sizes of cytosolic RNA by dynamic light scattering (DLS) (Fig. 5, H and I). Subjecting cells to osmotic stress caused a significant shift to larger sizes. Reducing PLCβ1 abundance resulted in a small peak at low molecular weights and a broad peak at larger sizes that was shifted to the right when compared to that for the control cells. This small peak was consistent with enhanced C3PO activity due to the relief of inhibition by PLCβ1 (*28*). Over-expressing $G\alpha_q$ resulted in a similar behavior as did treatment with siRNA(PLCβ1). As a control, we measured the DLS spectra of cytosolic RNA from untreated cells and in cells treated with the antibiotic puromycin, which halts mRNA translation, rendering mRNA in stress granules (*37*). The RNAs from puromycin-treated cells were almost two-fold greater in molecular weight compared to those in control cells and showed a small peak that corresponded to the sizes seen in control cells. These data (Fig. 5, H and

I) are consistent with the translational arrest and the accumulation of higher molecular weight RNAs that occurred when PLCβ1 abundance was reduced.

Cytosolic PLCβ1 abundance affects stress granules in smooth muscle cells

Myocytes and other cell types may experience changes in osmotic conditions during their lifetime. With this in mind, we extended our studies to two different smooth muscle cell types: rat aortic smooth muscle (A10) cells and Wistar-Kyoto rat 3M22 (WKO-3M22) cells. We identified PLCβ1-associated proteins in A10 cells under control conditions and after 5 min of osmotic stress by pulling down PLCβ1 complexes with a monoclonal antibody and identifying the proteins by MS analysis (table. S6). A large fraction of the proteins pulled down with PLCβ1 are associated with transcription, which is most likely due to the nuclear population of PLCβ (*38*). The stress granule–associated proteins were less abundant than the transcription-associated proteins. Many of the stress granule–associated proteins were also found in PC12 cells, for example, PABPC1 and eIF5A (Fig. 6A), whereas others, such as Ago2 and FXR, were not detected. We repeated these experiments with A10 cells that had been subjected to hypo-osmotic stress for 5 min before undergoing lysis. We detected a loss of almost all of the transcription-associated proteins and most of the stress granule–associated proteins (Fig. 6B). These results suggest that PLCβ1 binds to stress granule–associated proteins in A10 cells, as well as in PC12 cells, and that osmotic stress results in their release from PLCβ1. Whereas the cellular amount of PLCβ1 in A10 cells was reduced by osmotic stress, this effect was much lower than that in PC12 cells (fig. S7).

We then measured the formation of PABPC1 particles in A10 cells in which the cytosolic abundance of PLCβ1 was perturbed, such as by osmotic stress, siRNA(PLCβ1) treatment, and $G\alpha_q$

stimulation (Fig. 6, C to E). These cells exhibited particles that were ~10-fold larger than those in PC12 cells. Similar to PC12 cells, reducing PLCβ1 abundance in the A10 cells resulted in the formation of larger particles, which also occurred because of osmotic stress. In addition, stimulation with carbachol (to activate $G\alpha_q$) also resulted in a significant increase in the number of larger particles. Together, these data indicate that the size and number of PABPC1-containing particles depend on the abundance of PLCβ1 in the cytosol.

Both osmotic stress and carbachol also promoted the formation of Ago2-containing particles in WKO-3M22 cells. We analyzed the N&B results of these cells subjected to osmotic stress, carbachol stimulation (Fig. 7 A to C), and arsenite (fig. S10). As occurred with PC12 cells, both osmotic stress and carbachol stimulation promoted Ago2 aggregation in the WKO-3M22 cells, whereas arsenite stress had only a minor effect (fig. S10). Reducing the abundance of PLCβ1 promoted Ago2 aggregation in both control (Fig. 7, D and E) and arsenite-stressed cells (fig. S10). In a final series of experiments, we monitored shifts in the sizes of cytosolic RNA in WKO-3M22 cells subjected to osmotic stress or carbachol stimulation and found statistically significant increases in the RNA sizes under both conditions (Fig. 7F). Note that the particles and cytosolic RNAs in WKO-3M22 cells appeared to be larger than those found in PC12 cells (Fig. 5 versus Fig. 7).

Stress granule formation depends on the abundance of PLCβ1

To understand the dependence of stress granule formation on the abundance of PLCβ1, we assumed that eIF5A was the primary contact between PLCβ1 and stress granule–associated

proteins; however, eIF5B or another factor might be involved. We can then express the partitioning of eIF5A from the cytosol (c) to the particulate phase (p) as:

$$Kp = \frac{eIF5A^p}{eIF5A^c}$$

where $eIF5A^p$ is the stress granule phase, also termed *G*. The total amount of eIF5A is given by:

$E_T = eIF5A^p + eIF5A^c$,

where $eIF5A^c = eIF5^{free} + eIF5A\text{-}PLC\beta$.

We can then express the association between PLCβ and eIF5A in terms of a bimolecular dissociation constant:

$$K_d = \frac{[PLC\beta][eIF5A]}{[PLC\beta - eIF5A]}$$

In this equation, PLCβ refers to cytosolic PLCβ. We only considered the cytosolic population and not the membrane-bound population in accordance with our results showing that the loss of cytosolic PLCβ appeared to promote stress granule formation. Thus, the total cytosolic amount of PLCβ is given by:

$P_T = PLC\beta^{free} + PLC\beta\text{-}eIF5A$

If we combine these equations to determine the relationship between the number of particles and the concentration of PLCβ, we obtain an equation that is quadratic in *G* (eIF5A).

$$G^2\left(1+\frac{1}{K_p}\right)+G\left(P_T-E_T+K_pK_d+K_d\right)-K_pK_dE_T=0$$

To give:

$$G = \frac{-\left(P_T-E_T+K_d\left(1+K_p\right)\right)\pm\sqrt{P_T^2+E_T^2+K_d^2\left(1+K_p\right)^2+2K_d\left(1+K_p(P_T+E_T)\right)-2P_TE_T}}{\left(\frac{2\left(1+K_p\right)}{K_p}\right)}$$

To determine the applicability of this model, we first needed to estimate values for *G*. We found a linear dependence between the number of particles and the average area of the particles for PABPC1 in PC12 and in A10 cells (Fig. 8, A and B). This linearity enabled us to estimate *G* using either of these measurements. Note that this linearity did not occur for Ago2-containing particles for which stress primarily increased the number of particles rather than their size (Fig. 4).

We could estimate the total amount of cytosolic PLCβ by single molecule fluorescence measurements comparing the intensity of eYFP-PLCβ1 to an intensity scale constructed with Alexa488 as measured with a multiphoton laser in an fluorescence correlation instrument (see Materials and Methods). Briefly, we measured the number of eYFP-PLCβ1 molecules diffusing

in a specific confocal volume after calibration with Alexa488. Note that we typically over-express ~two-fold more protein as indicated by Western blotting analysis. Our measurements enabled us to estimate a cytosolic eYFP-PLCβ1 concentration of ~43 nM in PC12 cells and ~49 nM in A10 cells, which was reduced to 10 to 15 nM under hypo-osmotic conditions. This decline can be compared with the ~2.5-fold reduction in cytosolic PLCβ1 abundance that occurred in response to carbachol stimulation (Fig. 8B) and the 80 to 90% reduction in PLCβ1 abundance caused by siRNA treatment as seen in S9. Although these values for PLCβ1 are approximate, we used them to determine its dependence on stress granules as expressed as G^2. These data (Fig. 8C) showed the dependence of the size and number of stress granules when cyotsolic changes of PLCβ1 abundance occur.

DISCUSSION

The experiments presented here support the idea that cells direct signals through the reversible sequestration of proteins in membrane-less organelles. In some cases, these structures promote protein-protein interactions by reducing the local concentration and mobility of the proteins, whereas in other cases they effectively halt a functional pathway (*39, 40*). In this work, we showed that the atypical cytosolic population of PLCβ1 organized particles containing stress granule proteins in response $G\alpha_q$ signals. The specific types of stress granules that resulted from $G\alpha_q$-PLCβ1 signals appeared to be similar to those that occurred under osmotic stress but were distinct from those resulting from cold or heat shock, oxidative stress, or arsenite treatment. Our findings suggest that PLCβ1 regulates the entry of Ago2 and other stress granule proteins into particulates through a simple thermodynamic binding mechanism that is competitive with $G\alpha_q$ and that is dependent on the cytosolic concentration of PLCβ.

The traditional function of PLCβ is to generate Ca^{2+} signals in response to signaling molecules that lead to the activation of $G\alpha_q$, such as acetylcholine, dopamine, serotonin, melatonin, histamine, and angiotensin II. Note that without $G\alpha_q$ stimulation, the enzymatic activity of PLCβ1 is very low, and because $G\alpha_q$ resides at the plasma membrane and is not found in the cytosol, cytosolic PLCβ1 is not expected to be a substantial modifier of inositol phospholipids in internal membranes. Thus, any effect of these cytosolic binding partners on the enzymatic function of PLCβ1 would be immaterial; however, their ability to regulate its access to $G\alpha_q$ may be important for Ca^{2+} generation.

PLCβ1 plays multiple roles in cellular functions that are usually attributed to its enzymatic function. Studies showed that PLCβ1 can localize to the nucleus to regulate cell growth and differentiation, possibly through modulation of PIP_2 abundance in the nuclear envelope (*41, 42*). We previously found that a stable, cytosolic population of PLCβ1 affects various cell functions, such as RNA silencing and neuronal cell differentiation and proliferation independently of its catalytic activity (*43, 44*). These alternative cytosolic functions of PLCβ only occur at specific and limited times in the cell cycle. For this reason, we set out to determine whether cytosolic PLCβ1 binds to other proteins in nondifferentiating cells under nonstimulated conditions. With these parameters in mind, we used a proteomics approach to uncover potential interacting proteins and validated some of these interactions in live cells. Our experiments showed that under basal conditions, cytosolic PLCβ1 interacted with stress granule–associated proteins in intact cultured cells.

Stress granules are RNA-protein aggregates that enable cells to halt the translation of mRNAs encoding nonessential proteins when the cells are subjected to environmental stress. We found that many of the proteins that associated with PLCβ1 in complexes directly contribute to RNA-processing and ribosome assembly, and that these proteins were found in PLCβ1-containing complexes isolated from PC12 cells and A10 cells. During the initiation stage of mRNA translation, the polyadenylate binding protein PABP binds to the tail of the mRNA, which then associates with eIF4, enabling the mRNA-protein complex to bind to the 40*S* subunit (*45*). A cytosolic form of PABP, PABPC1, was found in our PLCβ1 pulldown assay together with eIF4 subtypes, which bind to PABPC1 (see https://www.uniprot.org/uniprot/P11940). Several other eIF proteins were also identified in our analysis.

An important step in the progression of translation is the hydrolysis of GTP on eIF2, which is catalyzed by the GTPase activity of eIF5. Our results suggest that eIF5A may be a primary binding partner to mediate the association of PLCβ1 with stress granule proteins. eIF5A is found at very high abundance in cells arrested at the G2/M checkpoint when protein translation is expected to be low. eIF5A has several regions in its sequence that are homologous to those of $G\alpha_q$, including a region through which $G\alpha_q$ directly binds to PLCβ (amino acid residues 147 to 162), as indicated by homologous sequence alignment and chemical cross-linking (*46*). We directly tested the association between PLCβ1 and eIF5A in experiments with purified proteins. Not only was the PLCβ1-eIF5A binding affinity in the same range as the affinity between PLCβ1 and C3PO (*15*), but the binding was competitive both in solution and in cells. Because the site in PLCβ1 through which it binds to C3PO overlaps with its binding site for $G\alpha_q$, the association of PLCβ1 with eIF5A should depend on the extent of $G\alpha_q$ activation, and this behavior was observed in our experiments.

Thus, in the absence of $G\alpha_q$ stimulation, a population of cytosolic PLCβ1 may associate with eIF5A until specific events, such as cellular differentiation, cause PLCβ1 binding to shift to C3PO and inhibit RNA-induced silencing.

We found that cytosolic PLCβ1 also bound to Ago2 as seen in our pull-down studies, co-immunoprecipitation experiments, and FRET/FLIM analysis. Our ability to disrupt the PLCβ1-Ago2 interaction by the addition of purified eIF5A is suggestive of a direct interaction. Ago2 is the key nuclease component of the RISC (*47*), and our previous work suggested an association between PLCβ1 and Ago2 (*14*). Sequence alignment of Ago2 and the TRAX subunits of C3PO shows four homologous regions ranging from ~20 to 40 amino acid residues in length and from 21 to 30% identity and 40 to 56% homology (residues 2 to 54, 87 to 119, 202 to 228, and 109 to 136 in C3PO and residues 788 to 826, 555 to 598, 188 to 202, and 831 to 858 in Ago2). Note that at least three of the C3PO regions are potential interaction sites for binding to PLCβ1, and at least one of these may be available for binding to PLCβ1-Ago2 (*28*). By this argument, it is possible that PLCβ1 directly binds to Ago2 through interactions similar to those through which it binds to C3PO.

We determined whether PLCβ1 affected stress granule formation by monitoring the behavior of two established stress granule markers, Ago2 and PABPC1. We initially used mild osmotic stress that may occur physiologically. Hypo-osmotic stress initiates a series of cellular events to reduce the number of osmolytes in the cell, such as the synthesis of glycogen from glucose, as well as ion flow (*48*). Whereas we expected osmotic strength to change the ability of PLCβ1 to interact with stress granule proteins by causing changes in tertiary or quaternary structure, we were surprised to

find a large reduction in PLCβ1a abundance in PC12 cells when osmotic stress was initially applied, although this effect was far less pronounced in A10 cells. The PLCβ1a and PLCβ1b isoforms differ by ~20 amino acids in the C-terminal region, but they are similarly activated by $G\alpha_q$. Piazzi *et al*. found that PLCβ1b, but not PLCβ1a, prevents cell death under oxidative conditions by affecting the amounts of key signaling proteins (*49*). Additionally, these two PLCβ1 isoforms may localize differently depending on cell type (*32-35, 50, 51*). Whereas our experiments could not adequately distinguish between these two isoforms, it would be interesting to investigate any separate roles they may play in stress granule formation. Note that in addition to the changes in PLCβ1 abundance or properties that occurred because of osmotic stress, we also varied cytosolic PLCβ1 abundance by stimulating $G\alpha_q$ to recruit PLCβ1 from the cytosol to the plasma membrane, and we also reduced total PLCβ1 abundance with siRNA(PLCβ1). All of these methods showed a connection between cytosolic PLCβ1 abundance and the formation of particles.

Our experiments showed that the stress granules formed by osmotic stress differed from those formed in response to other stresses. Whereas we observed a substantial assembly of Ago2 under osmotic stress, we found that arsenite, oxidative stress, and temperature shock produced particles that contained monomeric Ago2. In addition, osmotic stress resulted in a large increase in the size distribution of cytosolic RNAs, whereas arsenite, oxidative stress, and temperature shock did not. Studies in *S. cerevisiae* (*3*) indicate that hypo-osmotic stress promotes the formation of particles composed of markers of both P-bodies and stress granules, supporting our findings that subjecting mammalian cells to hypo-osmotic stress forms particles with compositions that differ from those formed in response to other types of stress. Our results also suggest that these latter granules, which have low Ago2 content and are rich in proteins associated with RNA-processing, such as G3BP,

are poised to prevent the translation of mRNAs whose protein products would not survive arsenite stress or oxidation, such as those involved in phosphorylation (*52*). In contrast, Ago2-rich granules, whose formation is mediated by the $G\alpha_q$-PLCβ1 pathway, may shift translation to mRNAs whose protein products enable cells to better respond to external signals. Thus, unlike arsenite or other stresses, $G\alpha_q$ activation may give rise to more physiologically relevant particles.

We monitored the appearance of stress granules under hypo-osmotic conditions structurally by fluorescence imaging and functionally by the accumulation of large cytosolic RNAs. Wheeler *et al*. showed that initially, stress granules are small and grow in size in a time-dependent manner (*5*). Here, we resolved particles greater than 10 μm^2 in area that formed in the cytoplasm, and the size and number of these particles did not vary between 5 and 10 min after stress induction. Additionally, whereas a very small population of eGFP-PLCβ1 incorporated into particles of ~400 μm^2, these were unchanged under conditions of osmotic stress, suggesting that PLCβ1 might deliver proteins into particles without incorporating into them. PABPC1 was associated with a high number of aggregates whose numbers were affected by the abundance of cytosolic PLCβ1 as determined by immunofluorescence analysis. Formation of Ago2-associated particles, as monitored by both immunofluorescence and live-cell imaging, was sensitive to $G\alpha_q$ stimulation but not to other stresses. Furthermore, the formation of stress granules associated with G3BP1, which did not appear to bind directly to PLCβ1, appeared to be sensitive to cytosolic PLCβ1 abundance and showed extensive and diffuse aggregation. These data suggest that cells respond to $G\alpha_q$ activation by sequestering Ago2, G3BP1, and other proteins into stress granules to halt the production of specific proteins.

Our results also suggest that the stress granules generated by $G\alpha_q$ activation are more similar to those formed by reducing PLCβ1 abundance or inducing osmotic stress in terms of Ago2 aggregates and are distinct from those produced by thermal or oxidative stress. Specifically, cold, heat, oxidative, or arsenite stress did not result in Ago2 aggregation and did not substantially affect the sizes of cytosolic RNAs, even though oxidative stress reduced the abundance of PLCβ1 together with that of many cellular proteins (*53*). Our results are consistent with the variability of stress granule composition formed in response to different types of stress (*37, 54, 55*). Our studies also suggest that a loss of cytosolic PLCβ1 may arrest the translation of mRNAs for specific proteins by promoting the formation of mRNA-Ago2–associated stress granules. The idea that sustained $G\alpha_q$ activation can regulate the production of specific proteins is intriguing and a comprehensive study of all of the transcripts affected by PLCβ1 is underway.

Neurons and cardiomyocytes are long-lived cells, and their viability depends on the reversible assembly of stress granules. We used PC12 cells as a model for the role of stress granules in neurological diseases and A10 cells as a model for muscle cells that regularly experience changes in osmolarity. We also used WYK-3M22 rat aortic smooth muscle cells as another model of muscle cells, which is used as the normotensive control for spontaneously hypertensive rats, which are a common model of hypertension (*56*). We found a similar set of stress-related proteins in PLCβ1-containing complexes in the two cell lines, with the exception of neural-specific proteins and RISC proteins, such as Ago2 and C3PO. Thus, PLCβ1 may serve a similar role in many cell types by mediating stress granule formation but not in regulating RNA processing.

We constructed a simple thermodynamic model in which the partitioning of eIF5A into particulates is regulated by its association with PLCβ1, but we note that eIF5A can easily be replaced with Ago2. The expression derived from this model shows the scope by which PLCβ1 could affect stress granule formation. Specifically, if the total amount of eIF5A is much greater than that of PLCβ1, then stress granule formation will be independent of PLCβ1. Considering the high concentration of ribosomes in cells, it is difficult to estimate the amount of eIF5A that would be available to bind to PLCβ1. We know that microinjection studies that delivered ~10 nM eIF5A into cells resulted in the displacement of C3PO from PLCβ1, which can give us a quantitative handle for future studies. Regardless of the specific nature of eIF5A and its associated proteins, our data suggest that there is a concentration range of PLCβ1 that sensitizes cells to stress granule formation and that this range is under the control of $G\alpha_q$ activation. Additionally, endogenous amounts of PLCβ1 may help to control premature stress responses.

In summary, our studies suggest a model in which cytosolic PLCβ1 binds to stress granule protein complexes to keep these proteins disperse under basal conditions. Activation of $G\alpha_q$ shifts the cytosolic population of PLCβ1 to the plasma membrane, displacing stress granule proteins and promoting the formation of particles. This dynamic nature of PLCβ1 is consistent with FCS studies showing the rapid movement of the enzyme between the cytosol and plasma membrane (*28*). We propose a model (Fig. 9) in which cells use cytosolic PLCβ1 abundance to regulate the formation and timing of protein synthesis and to prevent the formation of irreversible aggregates. Note that the quenching of $G\alpha_q$-PLCβ1–dependent Ca^{2+} signals in cells under osmotic stress suggests that the stress granules may effectively block this signaling pathway.

We previously found that PLCβ1 plays an important but uncharacterized role in neuronal cell development. Specifically, the expression of PLCβ1a increases substantially within the first 24 hours of PC12 cell differentiation and then slowly decreases (*16*), leading to the question of why its abundance is so variable. PLCβ1 is highly expressed in neuronal tissue in which dysfunction in stress granule assembly has been implicated in disease (*57, 58*). Our data suggest that PLCβ1 may act as a chaperone to keep stress granule proteins dispersed under basal conditions. Note that reductions in the amount PLCβ1 are associated with a host of neurological disorders that may result from disruptions in Ca^{2+} signaling and the proliferation and differentiation of neuronal cells (*59-62*). Schizophrenia and suicide specifically involve varying amounts of PLCβ1a and PLCβ1b in the prefrontal cortex (*61*). Note also that the PLCβ1-associated proteins identified here play important roles in neuronal function. FXR proteins are associated with the most common form of hereditary mental retardation (*63, 64*), whereas eIF5A is associated with neuronal growth and brain development (*65*). It is interesting to speculate about connections between PLCβ1-associated neurological disorders and those associated with FXR and eIF5A, which may involve dysfunction in stress granule assembly and disassembly.

MATERIALS AND METHODS

Cell culture

Rat phenochromocytoma (PC12) and rat aortic smooth muscle (A10) cells were obtained from ATCC. Wistar-Kyoto rat 3M22 (WKO-3M22) cells, originally obtained from ATCC, were a generous gift from M. Rolle (Department. of Biomedical Engineering, Worcester Polytechnic Institute). PC12 cells were cultured in high-glucose DMEM (GIBCO) with 10% heat-inactivated horse serum (GIBCO) and 5% fetal bovine serum (FBS, Atlanta Biologicals). A10 cell lines were

cultured in high-glucose DMEM with 10% FBS and 1% sodium pyruvate. WKY-3M22 cell lines were cultured in high-glucose DMEM (Corning) without L-glutamine with 10% FBS, 1% sodium pyruvate, 1% non-essential amino acids (VWR), and 1% L-glutamine (VWR). All cells were incubated at 37°C in 5% CO_2. Cells were synchronized in the G2/M phase as described previously (*17*). Briefly, 2 mM thymidine was added to the cells for 24 hours, after which the medium was removed and replaced by fresh complete culture medium for 8 hours, which was followed by the addition of nocodazole (40 ng/ml).

Plasmids

The EGFP-hArgonaute-2 (eGFP-Ago2) plasmid was purchased from (Addgene plasmid # 21981) and was prepared in the laboratory of Philip Sharp (MIT). The mCherry-Ago2 plasmid was a gift from Alissa Weaver (Vanderbilt University). EGFP-G3BP1 was purchased from Addgene (plasmid # 119950) and was prepared in the laboratory of Jeffrey Chao (Friedrich Miescher Institute). The mCherry-TRAX-C1 plasmid was constructed by inserting the cDNA encoding *TRAX* between the Bam HI and Eco RI restriction sites in the mCherry-C1 backbone with T4 DNA ligase (NEB). Cell transfections with plasmids and siRNAs were performed with Lipofectamine 3000 (Invitrogen) in antibiotic-free medium. The culture medium was changed to one containing antibiotic (1% Penicillin/Streptomycin) 12 to 18 hours after transfection. For every FLIM experiment, two separate samples were prepared: donor alone and donor in the presence of acceptor.

Co-immunoprecipitations

PC12 cells were lysed in buffer containing 1% Triton X-100, 0.1% SDS, 1x protease inhibitor cocktail, and 10 mM Tris (pH 7.4), after which 200 µg of soluble protein was incubated with 2 µl of anti-PLCβ1 or anti-Ago2 antibody overnight at 4°C. After the addition of 20 mg of protein A-Sepharose 4B beads (Invitrogen), the mixture was gently rotated for 4 hours at 4°C. Beads were washed three times with lysis buffer, and bound proteins were eluted with sample buffer for 5 min at 95°C. Precipitated proteins were loaded onto two 10% polyacrylamide gels. After SDS-PAGE, one gel was transferred to nitrocellulose membranes and proteins were detected by Western blotting analysis with anti-PLCβ1 (D-8, Santa Cruz) and anti-Ago2 (Abcam ab32381 Lot# GR3195666-1) antibodies.

Application of stress conditions

For hypo-osmotic stress conditions, the culture medium was diluted with 50% water for 5 min before it was removed and replaced with Hanks' Balanced Salt Solution (HBSS) for imaging. For the arsenite treatment, a stock solution of 100 mM arsenite in water was prepared. Cells were exposed to a final concentration of 0.5 mM arsenite for 10 min before the medium was removed and replaced by HBSS for imaging. For heat shock conditions, cells were incubated at 40°C for 1 hour, whereas for cold-shock, cells were incubated at 12°C for 1 hour. For the oxidative stress treatment, a stock solution of 1 M $CoCl_2$ was prepared, and the cells were exposed to a final concentration of 1 mM $CoCl_2$ for 12 to 16 hours (overnight) at 37ºC before the medium was removed. Treatment of both PC12 cells and WKO-3M22 cells with puromycin (20 µg/l) was performed for 30 min at 37ºC.

FRET studies between purified PLCβ1 and eIF5A

PLCβ1 was purified by over-expression in HEK293 cells as previously described (*29*). Purification of eIF5A was performed as described previously (*27*). Purified eIF5A in a pET28-mhl vector was expressed in bacteria (Rosetta 2 DE3 plysS) by inoculating 100 ml of an overnight culture grown in Luria-Bertani medium into 2 L of Terrific Broth medium in the presence of kanamycin (50 μg/ml) and chloramphenicol (25 μg/ml) at 37°C. When the culture reached an optical density at 600 nm (OD 600) of ~3.0, the temperature of the medium was reduced to 15°C and the culture was treated with 0.5 mM IPTG to induce protein production. The cells were allowed to grow overnight before they were harvested and stored at -80°C. Frozen cells from 1.8 L of TB culture were thawed, resuspended in 150 ml of lysis buffer [20 mM HEPES (pH 7.5), 300 mM NaCl, 5% glycerol, 2 mM β-mercaptoethanol (BME), 5 mM imidazole, 0.5% CHAPS, protease inhibitor cocktail, and 5 μl of DNAase), and lysed with a panda homogenizer. The lysate was centrifuged at 30,000*g* for 45 min, added to a cobalt column in binding buffer [20 mM HEPES (pH 7.5), 300 mM NaCl, 5% glycerol, 2 mM BME, 5 mM imidazole], and equilibrated in 4 x 1 mL of a 50% slurry of cobalt resin. We passed 150 ml of supernatant through each cobalt column at approximately 0.5 ml/min, washed first with 20 mM HEPES (pH 7.5), 300 mM NaCl, 5% glycerol, 2 mM BME, 30 mM imidazole, and second with 20 mM HEPES (pH 7.5), 300 mM NaCl, 5% glycerol, 2 mM BME, 75 mM imidazole, and eluted with 20 mM HEPES (pH 7.5), 300 mM NaCl, 5% glycerol, 2 mM BME, 300 mM imidazole. Protein-protein associations were assessed by FRET using sensitized emission. Briefly, PLCβ1a and eIF5A were covalently labeled on their N-termini with Alexa Fluor 488 and Alexa Fluor 594 (Invitrogen), respectively, and the increase in acceptor emission when the samples were excited at the donor wavelength in the presence of Alexa Fluor 488–PLCβ1 was measured. Studies were repeated by pre-binding catalytically inactive C3PO with Alexa Fluor 488–PLCβ1.

MS analysis

MS measurements were performed at the University of Massachusetts Medical School as previously described (*66*). Cytosolic fractions were isolated from cells, and proteins that bound to monoclonal anti-PLCβ1a antibody (Santa Cruz, D-8) were separated by electrophoresis. Protein bands were isolated by cutting the gels into 1x1-mm pieces, which were placed in 1.5-ml eppendorf tubes with 1 ml of water for 30 min. The water was removed, and 200 µl of 250 mM ammonium bicarbonate were added. Disulfide bonds were reduced by incubation with DTT at 50ºC for 30 min, which was followed by the addition of 20 µl of 100 mM iodoacetamide for 30 min at room temperature. The gel slices were washed twice with 1-ml water aliquots. The water was then removed, 1 ml of 50:50 50 mM ammonium bicarbonate:acetonitrile was placed in each tube, and the samples were incubated at room temperature for 1 hour. The solution was then removed and 200 µl of acetonitrile was added to each tube, at which point the gel slices turned white and became opaque. The acetonitrile was removed, and the gel slices were further dried in a Speed Vac (Savant Instruments, Inc.). Gel slices were rehydrated in 100 µl of sequencing-grade trypsin (4 ng/µl, Sigma) in 0.01% ProteaseMAX Surfactant (Promega): 50 mM ammonium bicarbonate. Additional bicarbonate buffer was added to ensure complete submersion of the gel slices. Samples were incubated at 37°C for 18 hours. The supernatant of each sample was then removed and placed into a separate 1.5-ml eppendorf tube. Gel slices were further extracted with 200 µl of 80:20 acetonitrile:1% formic acid. The extracts were combined with the supernatants of each sample. The samples were then completely dried down in a Speed Vac. Tryptic peptide digests were reconstituted in 25 µl of 5% acetonitrile containing 0.1% (v/v) trifluoroacetic acid and separated on a NanoAcquity (Waters) UPLC. Briefly, a 2.5-µl injection was loaded in 5% acetonitrile

containing 0.1% formic acid at 4.0 µl/min for 4.0 min onto a 100-µm inner diameter (I.D.) fused-silica pre-column packed with 2 cm of 5-µm (200 Å) Magic C18AQ (Bruker-Michrom) and eluted with a gradient at 300 nl/min onto a 75-µm I.D. analytical column packed with 25 cm^3 of 3-µm (100 Å) Magic C18AQ particles to a gravity-pulled tip. The solvents used were solvent A [water (0.1% formic acid)] and solvent B [acetonitrile (0.1% formic acid)]. A linear gradient was developed from 5% solvent A to 35% solvent B in 90 min. Ions were introduced by positive electrospray ionization through a liquid junction into a Q Exactive hybrid mass spectrometer (Thermo). Mass spectra were acquired over m/z 300 to 1750 at 70,000 resolution (m/z 200) and data-dependent acquisition selected the top 10 most abundant precursor ions for tandem mass spectrometry by HCD fragmentation using an isolation width of 1.6 Da, a collision energy of 27, and a resolution of 17,500. Raw data files were peak-processed with Proteome Discoverer software (version 2.1, Thermo) before undergoing database searching with Mascot Server (version 2.5) against the Uniprot_Rat database. Search parameters included trypsin specificity with two missed cleavages or no enzymatic specificity. The variable modifications of oxidized methionine, pyroglutamic acid for N-terminal glutamine, phosphorylation of serine and threonine, N-terminal acetylation of the protein, and a fixed modification for carbamidomethyl cysteine were considered. The mass tolerances were 10 ppm for the precursor and 0.05 Da for the fragments. Search results were then loaded into the Scaffold Viewer (Proteome Software, Inc.) for peptide/protein validation and label-free quantitation. These data were analyzed using percentage of total spectra in Scaffold4 software before plotting with Sigma Plot 14.

N&B measurements

N&B theory and measurement were fully described previously (*36*). Experimentally, we collected ~100 cell images in which we viewed either free eGFP (control) or eGFP-Ago2 at a 66 nm/pixel resolution and at a rate of 4 μs/pixel. Regions of interest (256x256 box) were analyzed from a 320x320 pixel image. Offset and noise were determined from the histograms of the dark counts performed every two measurements. N&B data were analyzed with SimFC software (www.lfd.uci.edu).

N&B analysis

N&B defines the number of photons associated with a diffusing species by analyzing the variation of the fluorescence intensity in each pixel in the cell image. In this analysis, the apparent brightness, B, in each pixel is defined as the ratio of the variance, σ, over the average fluorescence intensity <k>:

$$B = \sigma 2/< k >.$$

and

$$< k >= \epsilon n$$

where n is the number of fluorophores. The determination of the variance in each pixel is obtained by rescanning the cell image ~100 times as described earlier. The average fluorescence intensity, <k>, is directly related to the molecular brightness, ε, in units of photons per second per molecule, and n. B can also be expressed as:

$$B = \epsilon + 1$$

The apparent number of molecules, N, is defined as:

$$N = \epsilon n\ /(\epsilon + 1)$$

Fluorescence lifetime imaging measurements (FLIM)

FLIM measurements were performed on the dual-channel confocal fast FLIM (Alba version 5, ISS Inc.) equipped with photomultipliers and a Nikon Eclipse Ti-U inverted microscope. A 60× Plan Apo (1.2 NA, water immersion) objective and a mode-locked, two-photon titanium-sapphire laser (Tsunami; Spectra-Physics) were used in this study. The lifetime of the laser was calibrated each time before experiments by measuring the lifetime of Atto 435 in water with a lifetime of 3.61 ns (Ref) at 80, 160, and 240 MHz. The samples were excited at 800/850 nm, and emission spectra were collected through a 525/50 bandpass filter. For each measurement, the data were acquired until the photon count was >300. Fluorescence lifetimes were calculated by allowing ω = 80 MHz:

$$\tau = \frac{S}{G * 2\pi * \omega}$$

Statistical analysis

Data were analyzed with the Sigma Plot 13 statistical packages, which included the student's *t* test and one-way analysis of variance (ANOVA).

Dynamic light scattering (DLS)

DLS measurements were performed on a Malvern Panalytical Zetasizer Nano ZS instrument. For these experiments, mRNA from PC12 cells was extracted with the Qiagen Mini Kit (Cat #: 74104)

according to the manufacturer's instructions. Before the mRNA was extracted, the cells were exposed to stress, treated with siRNA(PLCβ1a), or transfected with plasmid expressing constitutively active $G\alpha_qRC$ (*67*). For these measurements, approximately 50 µl of extracted mRNA in RNase-free water was added in a Hellma Fluorescence Quartz Cuvette (QS-3.00mm). Each sample was run three times for 10 min per run. Control samples were repeated six times, the PLCβ knockdown sample twice, and the $G\alpha_q$ over-expression sample once.

Particle analysis

Samples were imaged with a 100X/1.49 oil TIRF objective to microscopically count the number of particles per μm^2 formed under different conditions. For each condition, 10 to 20 cells were randomly selected, and z-stack measurements were taken (1.0 µm/frame). Analysis was performed with ImageJ and Fiji ImageJ software in two ways. First, each measurement was thresholded before analyzing, and the number of particles per frame per measurement was averaged. Second, all z-stack measurements were combined to generate a 3D image for each sample before analyzing the number of particles per sample and averaging the results. Both methods produced identical results.

Microinjection studies

Microinjection of a solution of 100 nM eIF5A into PC12 cells was performed with an Eppendorf Femtojet Microinjector mounted on Nikon Eclipse Ti-U inverted confocal microscope under 0.35 PSI pressure and 0.5 s per injection.

Immunofluorescence

Cells were fixed with 3.7% formaldehyde, permeabilized with 0.1% triton X-100 in PBS, and then blocked with 10% goat serum, 5% BSA, 50 mM glycine in PBS. Cells were then stained with the appropriate primary antibodies (Abcam), incubated for 1 hour, washed, and treated with a secondary antibody for 1 hour. After another wash, the cells were viewed on a Zeiss Meta 510 laser confocal microscope. Data were analyzed with Zeiss LSM software and Image J. The secondary antibodies used were Alexa Fluor 488–conjugated anti-rabbit antibody for Ago-2 and Alexa Fluor 647–conjugated anti-mouse antibody for PABPC1.

Ca^{2+} signal imaging

Single-cell Ca^{2+} measurements were performed by labeling the cells with Calcium Green (Thermofisher), incubating the cells in HBSS for 45 min, and then washing the cells twice with HBSS. The release of intracellular Ca^{2+} in live PC12 cells was initiated by the addition of 2 μM carbachol before imaging the time series on a Zeiss LSM 510 confocal microscope with excitation at 488 nm using the time series mode as previously described (*68*).

Western blotting analysis

Samples were placed in 6-well plates and collected in 250 μl of lysis buffer, which included NP-40 and protease inhibitors as mentioned earlier. Sample buffer was added at 20% of the total volume. After SDS-PAGE electrophoresis, proteins were transferred to nitrocellulose membranes (Bio-Rad). The primary antibodies used included: anti-PLCβ1 (Santa Cruz sc-5291), anti-Ago2 (abcam ab32381), anti-PABPC1 (Santa Cruz sc-32318), anti-G3BP1 (Santa Cruz sc-81940), anti-actin (abcam ab8226), anti-HSP90 (Santa Cruz sc-69703), anti-eGFP (Santa Cruz sc-8334) and siRNA PLCβ1 (Ambion 4390771). Membranes were treated with antibodies diluted 1:1000 in

0.5% milk and washed three times for 5 min each before applying the appropriate secondary antibody (anti-mouse or anti-rabbit, Santa Cruz) at a 1:2000 dilution. Membranes were washed three times for 10 min each before being imaged on a BioRad chemi-doc imager to determine the relative band intensities. Band intensities were measured at several sensitivities and exposure times to ensure that the intensities were in a linear range. Data were analyzed with ImageJ software.

SUPPLEMENTARY MATERIALS

Figs. S1 to S10.
Tables S1 to S6.

REFERENCES AND NOTES

1. P. Anderson, N. Kedersha, RNA granules. *J Cell Biol* **172**, 803-808 (2006); published online EpubMar 13 (10.1083/jcb.200512082).
2. D. S. W. Protter, R. Parker, Principles and Properties of Stress Granules. *Trends Cell Biol* **26**, 668-679 10.1016/j.tcb.2016.05.004).
3. K. H. Shah, S. N. Varia, L. A. Cook, P. K. Herman, A Hybrid-Body Containing Constituents of Both P-Bodies and Stress Granules Forms in Response to Hypoosmotic Stress in Saccharomyces cerevisiae. *PLoS One* **11**, e0158776 (2016)10.1371/journal.pone.0158776).
4. A. Khong, T. Matheny, S. Jain, S. F. Mitchell, J. R. Wheeler, R. Parker, The Stress Granule Transcriptome Reveals Principles of mRNA Accumulation in Stress Granules. *Molecular Cell* **68**, 808-820.e805 10.1016/j.molcel.2017.10.015).
5. J. R. Wheeler, T. Matheny, S. Jain, R. Abrisch, R. Parker, Distinct stages in stress granule assembly and disassembly. *eLife* **5**, e18413 (2016); published online Epub2016/09/07 (10.7554/eLife.18413).
6. P. Anderson, N. Kedersha, Stress granules. *Current Biology* **19**, R397-R398 10.1016/j.cub.2009.03.013).
7. M. Ramaswami, J. P. Taylor, R. Parker, Altered Ribostasis: RNA-Protein Granules in Degenerative Disorders. *Cell* **154**, 727-736 10.1016/j.cell.2013.07.038).
8. A. Detzer, C. Engel, W. Wunsche, G. Sczakiel, Cell stress is related to re-localization of Argonaute 2 and to decreased RNA interference in human cells. *Nucleic Acids Res* **39**, 2727-2741 (2011); published online EpubApr (10.1093/nar/gkq1216).
9. S. M. Hammond, A. A. Caudy, G. J. Hannon, Post-transcriptional gene silencing by double-stranded RNA. *Nat Rev Genet* **2**, 110-119 (2001); published online EpubFeb (
10. J. Lopez-Orozco, J. M. Pare, A. L. Holme, S. G. Chaulk, R. P. Fahlman, T. C. Hobman, Functional analyses of phosphorylation events in human Argonaute 2. *RNA* **21**, 2030-2038 (2015)10.1261/rna.053207.115).
11. P. Suh, J. Park, L. Manzoli, L. Cocco, J. Peak, M. Katan, K. Fukami, T. Kataoka, S. Yun, S. Ryu, Multiple roles of phosphoinositide-specific phospholipase C isozymes. *BMB reports* **41**, 415-434 (2008).
12. M. Rebecchi, S. Pentylana, Structure, function and control of phosphoinositide-specific phospholipase C. *Physiological Reviews* **80**, 1291-1335 (2000).

13. L. Dowal, P. Provitera, S. Scarlata, Stable association between G alpha(q) and phospholipase C beta 1 in living cells. *J Biol Chem* **281**, 23999-24014 (2006); published online EpubAug 18 (
14. F. Philip, Y. Guo, O. Aisiku, S. Scarlata, Phospholipase Cβ1 is linked to RNA interference of specific genes through translin-associated factor X. *The FASEB Journal* **26**, 4903-4913 (2012); published online EpubDecember 1, 2012 (10.1096/fj.12-213934).
15. O. R. Aisiku, L. W. Runnels, S. Scarlata, Identification of a Novel Binding Partner of Phospholipase Cβ1: Translin-Associated Factor X. *PLoS One* **5**, e15001 (2010).
16. O. Garwain, S. Scarlata, Phospholipase Cβ-TRAX Association Is Required for PC12 Cell Differentiation. *Journal of Biological Chemistry* **291**, 22970-22976 (2016); published online EpubOctober 28, 2016 (10.1074/jbc.M116.744953).
17. O. Garwain, K. Valla, S. Scarlata, Phospholipase Cβ1 regulates proliferation of neuronal cells. *The FASEB Journal* **In press**, fj.201701284R (2018)10.1096/fj.201701284R).
18. T. Yanagi, M. Krajewska, S.-i. Matsuzawa, J. C. Reed, PCTAIRE1 Phosphorylates p27 and Regulates Mitosis in Cancer Cells. *Cancer Research* **74**, 5795-5807 (2014)10.1158/0008-5472.can-14-0872).
19. T. Yanagi, S.-i. Matsuzawa, PCTAIRE1/PCTK1/CDK16: a new oncotarget? *Cell Cycle* **14**, 463-464 (2015); published online Epub2015/02/16 (10.1080/15384101.2015.1006539).
20. H. Mahboubi, U. Stochaj, Cytoplasmic stress granules: Dynamic modulators of cell signaling and disease. *Biochim Biophys Acta* **1863**, 884-895 (2017); published online EpubApr (10.1016/j.bbadis.2016.12.022).
21. O. Garwain, K. Valla, S. Scarlata, Phospholipase Cβ1 regulates proliferation of neuronal cells. *The FASEB Journal* **32**, 2891-2898 (2018)10.1096/fj.201701284R).
22. L. Cocco, A. M. Martelli, R. S. Gilmour, S. G. Rhee, F. A. Manzoli, Nuclear phospholipase C and signaling. *Biochim Biophys Acta* **1530**, 1-14 (2001); published online EpubJan 15 (
23. J. Lakowicz, *Principles of Fluorescence Spectroscopy, Second Edition*. (Plenum, New York, 1999).
24. M. A. Digman, V. R. Caiolfa, M. Zamai, E. Gratton, The Phasor Approach to Fluorescence Lifetime Imaging Analysis. *Biophysical Journal* **94**, L14-L16 (2008); published online Epub11/02

08/18/received

09/17/accepted (10.1529/biophysj.107.120154).
25. G. H. Patterson, D. W. Piston, B. G. Barisas, Forster distances between green fluorescent protein pairs. *Anal Biochem* **284** 438-440 (2000).
26. F. Philip, S. Sahu, U. Golebiewska, S. Scarlata, RNA-induced silencing attenuates G protein-mediated calcium signals. *Faseb j* **30**, 1958-1967 (2016); published online EpubMay (10.1096/fj.201500140).
27. F. E. Paulin, L. E. Campbell, K. O'Brien, J. Loughlin, C. G. Proud, Eukaryotic translation initiation factor 5 (eIF5) acts as a classical GTPase-activator protein. *Curr Biol* **11**, 55-59 (2001); published online EpubJan 9 (
28. S. Sahu, L. Williams, A. Perez, F. Philip, G. Caso, W. Zurawsky, S. Scarlata, Regulation of the activity of the promoter of RNA-induced silencing, C3PO. *Protein Science* **26**, 1807-1818 (2017)10.1002/pro.3219).
29. S. Sahu, F. Philip, S. Scarlata, Hydrolysis Rates of Different Small Interfering RNAs (siRNAs) by the RNA Silencing Promoter Complex, C3PO, Determines Their Regulation by Phospholipase Cβ. *Journal of Biological Chemistry* **289**, 5134-5144 (2014); published online EpubFebruary 21, 2014 (10.1074/jbc.M113.531467).
30. Y. Guo, L. Yang, K. Haught, S. Scarlata, Osmotic Stress Reduces Ca2+ Signals through Deformation of Caveolae. *J Biol Chem* **290**, 16698-16707 (2015); published online EpubJul 3 (10.1074/jbc.M115.655126).

31. L. Yang, S. Scarlata, Super-resolution Visualization of Caveola Deformation in Response to Osmotic Stress. *J Biol Chem* **292**, 3779-3788 (2017); published online EpubMar 03 (10.1074/jbc.M116.768499).
32. Y. Y. Bahk, Y. H. Lee, T. G. Lee, J. Seo, S. H. Ryu, P. G. Suh, Two forms of phospholipase C-beta 1 generated by alternative splicing. *Journal of Biological Chemistry* **269**, 8240-8245 (1994); published online EpubMarch 18, 1994 (
33. Y. Bahk, H. Song, K. J. Baek, B. Y. Park, H. Kim, S. H. Ryu, P. G. Suh, Localization of two forms of phospholipase Cβ1, a and b, in C6Bu-1 cells. *Biochem Biophys Acta* **1389**, 76-80 (1998).
34. C. G. Kim, D. Park, S. G. Rhee, The role of carboxyl-terminal basic amino acids in $G_q\alpha$-dependent activation, particulate association, and nuclear localization of phospholipase C-β_1. *J Biol Chem* **271**, 21187-21192 (1996); published online EpubAug 30 (
35. D. R. Grubb, O. Vasilevski, H. Huynh, E. A. Woodcock, The extreme C-terminal region of phospholipase Cbeta1 determines subcellular localization and function; the "b" splice variant mediates alpha1-adrenergic receptor responses in cardiomyocytes. *Faseb j* **22**, 2768-2774 (2008); published online EpubAug (10.1096/fj.07-102558).
36. M. A. Digman, R. Dalal, A. F. Horwitz, E. Gratton, Mapping the Number of Molecules and Brightness in the Laser Scanning Microscope. *Biophys J* **97**, 2320-2332 (2008).
37. A. Aulas, M. M. Fay, S. M. Lyons, C. A. Achorn, N. Kedersha, P. Anderson, P. Ivanov, Stress-specific differences in assembly and composition of stress granules and related foci. *J Cell Sci* **130**, 927-937 (2017); published online EpubMar 1 (10.1242/jcs.199240).
38. L. Cocco, I. Faenza, R. M. Fiume, S. R. Gilmour, F. A. Manzoli, Phosphoinositide-specific phospholipase C (PI-PLC) [beta]1 and nuclear lipid-dependent signaling. *Biochem Biophys Acta* **1761**, 509-521 (2006).
39. L. B. Case, X. Zhang, J. A. Ditlev, M. K. Rosen, Stoichiometry controls activity of phase-separated clusters of actin signaling proteins. *Science* **363**, 1093-1097 (2019)10.1126/science.aau6313).
40. W. Y. C. Huang, S. Alvarez, Y. Kondo, Y. K. Lee, J. K. Chung, H. Y. M. Lam, K. H. Biswas, J. Kuriyan, J. T. Groves, A molecular assembly phase transition and kinetic proofreading modulate Ras activation by SOS. *Science* **363**, 1098-1103 (2019)10.1126/science.aau5721).
41. L. Cocco, L. Manzoli, I. Faenza, G. Ramazzotti, Y. R. Yang, J. A. McCubrey, P. G. Suh, M. Y. Follo, Modulation of nuclear PI-PLCbeta1 during cell differentiation. *Adv Biol Regul* **60**, 1-5 (2016); published online EpubJan (10.1016/j.jbior.2015.10.008).
42. G. Ramazzotti, I. Faenza, R. Fiume, A. M. Billi, L. Manzoli, S. Mongiorgi, S. Ratti, J. A. McCubrey, P. G. Suh, L. Cocco, M. Y. Follo, PLC-beta1 and cell differentiation: An insight into myogenesis and osteogenesis. *Adv Biol Regul* **63**, 1-5 (2017); published online EpubJan (10.1016/j.jbior.2016.10.005).
43. S. Scarlata, O. Garwain, L. Williams, I. G. Burguera, B. Rosati, S. Sahu, Y. Guo, F. Philip, U. Golebiewska, Phospholipase Cbeta connects G protein signaling with RNA interference. *Adv Biol Regul* **61**, 51-57 (2016); published online EpubMay (10.1016/j.jbior.2015.11.006).
44. S. Scarlata, A. Singla, O. Garwain, Phospholipase Cβ interacts with cytosolic partners to regulate cell proliferation. *Advances in Biological Regulation*, (2017); published online Epub2017/09/09/ (https://doi.org/10.1016/j.jbior.2017.09.004).
45. B. Alberts, D. Bray, J. Lewis, M. Raff, K. Roberts, J. Watson, *Molecular Biology of the Cell*. (Garland, New York, 1994).
46. A. M. Lyon, V. M. Tesmer, V. D. Dhamsania, D. M. Thal, J. Gutierrez, S. Chowdhury, K. C. Suddala, J. K. Northup, J. J. G. Tesmer, An autoinhibitory helix in the C-terminal region of phospholipase C-β mediates Gαq activation. *Nat Struct Mol Biol* **18**, 999-1005 (2011)http://www.nature.com/nsmb/journal/vaop/ncurrent/abs/nsmb.2095.html#supplementary-information).

47. G. Hutvagner, M. J. Simard, Argonaute proteins: key players in RNA silencing. *Nature Reviews Molecular Cell Biology* **9**, 22 (2008); published online Epub01/01/online (10.1038/nrm2321).
48. K. Dietmar, Osmotic stress sensing and signaling in animals. *The FEBS Journal* **274**, 5781-5781 (2007)doi:10.1111/j.1742-4658.2007.06097.x).
49. M. Piazzi, W. L. Blalock, A. Bavelloni, I. Faenza, M. Raffini, F. Tagliavini, L. Manzoli, L. Cocco, PI-PLCβ1b affects Akt activation, cyclin E expression, and caspase cleavage, promoting cell survival in pro-B-lymphoblastic cells exposed to oxidative stress. *The FASEB Journal* **29**, 1383-1394 (2015)10.1096/fj.14-259051).
50. A. M. Martelli, R. S. Gilmour, V. Bertagnolo, L. M. Neri, L. Manzoli, L. Cocco, Nuclear localization and signalling activity of phosphoinositidase C beta in Swiss 3T3 cells. *Nature* **358**, 242-245 (1992); published online EpubJul 16 (
51. T. M. Filtz, D. R. Grubb, T. J. McLeod-Dryden, J. Luo, E. A. Woodcock, Gq-initiated cardiomyocyte hypertrophy is mediated by phospholipase Cβ1b. *The FASEB Journal* **23**, 3564-3570 (2009); published online EpubOctober 1, 2009 (10.1096/fj.09-133983).
52. M. F. Hughes, Arsenic toxicity and potential mechanisms of action. *Toxicol Lett* **133**, 1-16 (2002); published online EpubJul 7 (
53. Y. Guo, S. Scarlata, A Loss in Cellular Protein Partners Promotes α-Synuclein Aggregation in Cells Resulting from Oxidative Stress. *Biochemistry* **52**, 3913-3920 (2013); published online Epub2013/06/04 (10.1021/bi4002425).
54. J. Y. Youn, W. H. Dunham, S. J. Hong, J. D. R. Knight, M. Bashkurov, G. I. Chen, H. Bagci, B. Rathod, G. MacLeod, S. W. M. Eng, S. Angers, Q. Morris, M. Fabian, J. F. Cote, A. C. Gingras, High-Density Proximity Mapping Reveals the Subcellular Organization of mRNA-Associated Granules and Bodies. *Mol Cell* **69**, 517-532.e511 (2018); published online EpubFeb 1 (10.1016/j.molcel.2017.12.020).
55. S. Jain, Joshua R. Wheeler, Robert W. Walters, A. Agrawal, A. Barsic, R. Parker, ATPase-Modulated Stress Granules Contain a Diverse Proteome and Substructure. *Cell* **164**, 487-498 10.1016/j.cell.2015.12.038).
56. J. M. Lemire, C. W. Covin, S. White, C. M. Giachelli, S. M. Schwartz, Characterization of cloned aortic smooth muscle cells from young rats. *The American journal of pathology* **144**, 1068-1081 (1994).
57. B. Wolozin, Physiological Protein Aggregation Run Amuck: Stress Granules and the Genesis of Neurodegenerative Disease. *Discovery medicine* **17**, 47-52 (2014).
58. L. Chen, B. Liu, Relationships between Stress Granules, Oxidative Stress, and Neurodegenerative Diseases. *Oxidative Medicine and Cellular Longevity* **2017**, 10 (2017)10.1155/2017/1809592).
59. A. J. Hannan, P. C. Kind, C. Blakemore, Phospholipase C-β1 expression correlates with neuronal differentiation and synaptic plasticity in rat somatosensory cortex. *Neuropharmacology* **37**, 593-605 (1998); published online Epub4/5/ (http://dx.doi.org/10.1016/S0028-3908(98)00056-2).
60. C. E. McOmish, E. L. Burrows, M. Howard, A. J. Hannan, PLC-β1 knockout mice as a model of disrupted cortical development and plasticity: Behavioral endophenotypes and dysregulation of RGS4 gene expression. *Hippocampus* **18**, 824-834 (2008)10.1002/hipo.20443).
61. M. Udawela, E. Scarr, S. Boer, J. Y. Um, A. J. Hannan, C. McOmish, C. C. Felder, E. A. Thomas, B. Dean, Isoform specific differences in phospholipase C beta 1 expression in the prefrontal cortex in schizophrenia and suicide. *npj Schizophrenia* **3**, 19 (2017); published online Epub2017/04/19 (10.1038/s41537-017-0020-x).
62. H.-j. Kim, H.-Y. Koh, Impaired Reality Testing in Mice Lacking Phospholipase Cβ1: Observed by Persistent Representation-Mediated Taste Aversion. *PLoS One* **11**, e0146376 (2016)10.1371/journal.pone.0146376).

63. C. Agulhon, P. Blanchet, A. Kobetz, D. Marchant, N. Faucon, P. Sarda, C. Moraine, A. Sittler, V. Biancalana, A. Malafosse, M. Abitbol, Expression of FMR1, FXR1, and FXR2 genes in human prenatal tissues. *J Neuropathol Exp Neurol* **58**, 867-880 (1999); published online EpubAug (
64. B. Bardoni, A. Schenck, J.-L. Mandel, The Fragile X mental retardation protein. *Brain Research Bulletin* **56**, 375-382 (2001); published online Epub2001/11/01/ (https://doi.org/10.1016/S0361-9230(01)00647-5).
65. Y. Huang, D. S. Higginson, L. Hester, M. H. Park, S. H. Snyder, Neuronal growth and survival mediated by eIF5A, a polyamine-modified translation initiation factor. *Proceedings of the National Academy of Sciences of the United States of America* **104**, 4194-4199 (2007); published online Epub02/28

12/07/received (10.1073/pnas.0611609104).
66. S. Iwata, Lee, J.W., Okada, K., Lee, J.K. Iwata, M., Rasmussen, B., Link T.A., Ramaswamy, S. and Jap, B.K., Complete at of the 11 subunit bovine mitochondrial cytochrome bc1 complex. *Science* **281**, 64-71 (1998).
67. T. E. Hughes, H. Zhang, D. Logothetis, C. H. Berlot, Visualization of a functional Gαq-green fluorescent protein fusion in living cells. *J.Biol.Chem.* **276**, 4227-4235 (2001).
68. R. C. Calizo, S. Scarlata, A Role for G-Proteins in Directing G-Protein-Coupled Receptor–Caveolae Localization. *Biochemistry* **51**, 9513-9523 (2012)10.1021/bi301107p).
69. C. A. Royer, S. F. Scarlata, in *Methods in Enzymology*. (Academic Press, 2008), vol. 450, pp. 79-106.

Acknowledgments: The authors thank M. Rolle (WPI) for the WKO-3M22 cells and E. Bafaro (WPI) for her help in cloning mCherry-TRAX, S. Yerramilli (WPI) for help with the N&B experiments and his helpful comments throughout this work, and G. Fiorentino (WPI) for her help in gathering data. S.S. is also a Professor Emeritus at Stony Brook University, NY, USA. **Funding:** The authors are grateful for the support of NIH GM116187. O.G. was supported by a Richard Whitcomb Fellowship.. **Author contributions:** A.Q., L.J., and O.G. were involved in experimental design, data collection, and analysis; A.S. was involved in conceptualization and data collection; S.S. was involved in conceptualization, experimental design, data analysis, and writing the paper. **Competing interests:** The authors declare that they have no competing interests. **Data and materials availability:** All data needed to evaluate the conclusions in the paper are present in the paper or the Supplementary Materials.

Fig. 1. Major binding partners of PLCβ1 in PC12 cells. (**A** and **B**) Proteins associated with PLCβ1 were pulled down with a monoclonal antibody from the cytosolic fractions of unsynchronized PC12 cells primarily in the G1 phase (A) or PC12 cells arrested in the G2/M phase (B) and then subjected to MS analysis. The relative amounts of the indicated proteins were calcuated as described in Materials and Methods. All of the proteins identified in (A), except for eIF5B, were also found in an identical experiment in which proteins associated with Ago2 were

pulled down (table S4). Proteins that were found to be phosphorylated included (A) FXR2 and (B) eIF3A, eIF3B, and eIF3C. Data were gathered from a single set of MS measurements and key features were validated biochemically as described in the text. (**C** and **D**) The cytsolic fractions of undifferentiated PC12 cells that were untransfected (control) or were transfected to overexpress Ago2, TRAX, or constitutively active $G\alpha_q$ were incubated with a monoclonal anti-PLCβ1 antibody to pull down PLCβ1-associated proteins. The pull-down samples (10 μg) were then analzyed by Western blotting with antibodies against PLCβ1, PABC1, and Ago2, as indicated in the representative blots (fig.S1), and a compilation of the relative intensties of the bands of interest was determined by densitometry (see Materials and Methods). Data are means ± SD of eight experiments. $*P < 0.001$. The relative amounts of C3PO and $G\alpha_q$ that were pulled down with PLCβ1 were not significantly different from that of PABPC1: $P = 0.81$ and $P = 0.54$, respectively. (D) A similar study to that described in (C) was performed with a monoclonal anti-GFP antibody to isolate either eGFP-PLCβ1 or eGFP-G3BP1 and their associated proteins from whole transfected PC12 cells. The relative amounts of the indicated proteins that were pulled down were determined by densitometry. Data are means ± SD of five experiments for PLCβ1, PABPC1, and Ago2 and of two experiments for G3BP1. Full-sized Western blots for representative samples can be see in fig. S1.

Fig. 2. Binding of PLCβ1 to Ago2 and eIF5A in PC12 cells. (**A** to **C**) Representative phasor plots from transfected PC12 cells expressing (A) eGFP-PLCβ1 alone or (B) eGFP-PLCβ1 and mCherry-Ago2. The raw lifetimes are plotted in polar coordinates, as indicated from the phase and modulated fluorescence lifetimes (see Results). Each point in the phasor plots corresponds to the lifetime of the eGFP-PLCβ1 emission measured in each pixel from the corresponding cell image

shown in the graph. Images are representative of five to eight cells from three independent experiments. (C) A phasor diagram in which the non-FRET and FRET points are selected and the pixels are shown in the cell images. Note that no significant FRET was detected in control studies of eGFP-C3PO and mCherry-Ago2 (fig. S2). (**D**) Example of a phasor plot and the corresponding image from a FLIM measurement of eGFP-PLCβ1 expressed in a PC12 cell. The heat map indicates eGFP signal intensity. (**E**) A similar study to that described in (B) except that PC12 cells were cotransfected with plasmids expressing eGFP-PLCβ1 and mCherry-C3PO (TRAX). Purple dots indicate pixels represented in the phasor plot. (**F**) A similar study to that described in (E) except that this cell was microinjected with purifed, unlabeled eIF5A. (**G**) Compilation of eGFP-PLCβ1 lifetime results from two independent studies with n = 10 cells for each study and in which free mCherry was used as a negative control. Comparison of data before and after eIF5A microinjection was statistically significant: $^{**}P < 0.001$.

Fig. 3. The effect of osmotic stress on cytosolic PLCβ1 in PC12 cells. (**A**) Representative Western blotting analysis of the cytosolic fractions of PC12 cells for PLCβ1 where PLCβ1a is the upper band of the doublet and PLCβ1b is the lower band. Cells were subjected to 10 min of incubation with 5 μM carbachol to stimulate $G\alpha_q$ activity or were subjected to osmotic stress (150 mOsm) for 5 and 30 min. PABPC1 and β-tubulin bands are shown for comparison. (**B**) Results of a study in which undifferentiated PC12 cells transfeccted to express eGFP-PLCβ1 were subjected to osmotic stress as indicated, and changes in cytosolic fluorescence intensity in a slice in middle of the cell were quantified. Data are from nine independent experiments. Compared to control cells, those subjected to osmotic stress for 5 min had significantly different fluorescence intensity ($P < 0.001$). (**C**) Analysis of the change in Ca^{2+} release when PC12 cells labeled with Calcium

Green were stimulated with 5 μM carbachol under basal conditions (300 mOsm) and hypo-osmotic stress (150 mOsm) for 10 min. Data are from n = 12 cells from three experiments and bars indicate SD. (**D**) Images of PC12 cells immunstained for Ago2 (green) and PABPC1 (red) under basal conditions (control), when the osmolarity was lowered from 300 to 150 mOsm (osmotic stress), and when cells that had been treated with siRNA(PLCβ1) were subjected to normal conditions or osmotic stress. Scale bars, 20 μm. (**E**) Compiled colocalization data showing the extent of colocalization of PABPC1 and Ago2 in cells from the experiments shown in (D). Data are from three experiments with 20 cells per experiment. ***$P = 0.002$ and **** $P \leq 0.001$.

Fig. 4. The effect of PLCβ1 on the formation of PABPC1- and Ago2-associated particles in PC12 cells. (**A** to **C**) The sizes and numbers of particles associated with monoclonal anti-PABPC1 in the cytosol of fixed and immunostained PC12 cells were measured with a 100x objective and analyzed by Image J software (see Materials and Methods). (A) Treatment of cells with siRNA(PLCβ1) relative to mock-transfected controls. Inset: An enlarged version of the plot is shown to enable better comparison. (B) Analysis of the effect of osmotic stress (150 mOsm, 5 min) on the size and number of PABPC1-associated particles in control PC12 cells and in PC12 cells treated with siRNA(PLCβ1). (C) Analysis of the effect of $G\alpha_q$ stimulation by treatment with 5 μM carbachol on the size and number of PABPC1-associated particles in control PC12 cells and in PC12 cells treated with siRNA(PLCβ1). (**D** to **F**) Size and number of Ago2-associated particles as determined by immunofluorescence analysis with a monoclonal antibody of for cells that were treated with siRNA(PLCβ1) and compared to control cells (D). Control cells subjected to 5 min of osmotic stress (150 mOsm) were compared to cells treated with siRNA(PLCβ1) under osmotic stress (E). Control cells treated with 5 μM carbachol to stimulate $G\alpha_q$ were compared to cells

treated siRNA(PLCβ1) and stimulated with 5 μM carbachol (F). Data are an average of three independent experiments that each sampled 10 cells. Error bars represent SD. The *P* values compare control conditions to the specific condition and were determined by ANOVA.

Fig. 5. Aggregation of Ago2 and G3BP1 in PC12 cells as monitored by N&B analysis. (**A** to **G**) N&B studies of PC12 cells expressing eGFP-Ago2 (A to C) and eGFP-G3BP1 (D to G) and subjected to the indicated conditions. Top: The graphs display N&B values for each pixel where the y-axis corresponds to the brightness of the particle and the x-axis shows particle intensity. The pixels contained in the red boxes are the values found for free eGFP and correspond to monomeric eGFP-Ago2 (A to C) or eGFP-G3BP1 (D to G). Points outside the red boxes, shown in green and blue, correspond to higher-order species of Ago2 or G3BP1. Middle: Images show the pixels corresponding to monomeic (red) and higher-order eGFP-Ago2 or eGFP-G3BP1 aggregates (green and blue) from the data shown in the graphs directly above. Bottom: Images are from fluorescence microscopy analysis with ISS software. The purple pixels denote Ago2 or G3BP1 aggregates. Data in (A) and (D) show control cells (n = 8 experiments); data in (B) and (E) show cells subjected to hypo-osmotic stress (150 mOsm, 5 min) (n = 8 experiments); and data in (C) and (G) show cells subjected to carbachol stimulation (5 μM, 10 min) (n = 5 experiments). data in (F) show cells treated with siRNA(PLCβ1) (n = 4 Scale bars, 10 μm. (**H**) The size distribution of cytosolic RNAs isolated from the indicated PC12 cells was measured by dynamic light scattering for control conditions (black), hypo-osmotic stress (150 mOsm, 5 min, green), over-expression of constiutively active $G\alpha_q$ (blue), and treatment with siRNA(PLCβ1) (pink). Inset: DLS spectra of cytosolic RNAs extracted from control cells and from cells treated with puromyocin; the x-axis range is from 0 to 3000 nm. (**I**) The size distribution of cytosolic RNAs where data for control

cells (black) is included for easier comparison to cells subjected to hypo-osmotic stress (150 mOsm 5min, red), heat shock at 40°C for 1 hour (green), cold shock at 12ºC for 1 hour (blue), and treatment with 0.5 mM arsenite for 10 min (pink). Inset: A comparison of control and puromysin-treated cells. Note that no changes were observed in cells subjected to oxidative stress (treatment with 12 mM $CoCl_2$ for 8 hours; fig. S7). Normalized data are shown. Each sample was scanned three times with 10 minutes per run. The numbers of independent samples were six (control) and two (PLCβ1 knockdown,$G\alpha_q$ over-expression, heat shock, cold shock, arsenite) and four (hypo-osmotic stress).

Fig. 6. The effect of PLCβ1 on stress granule formation in A10 cells. (**A** and **B**) MS analysis of the proteins associated with PLCβ1 in A10 cells under normal osmotic conditions (A) and after being subjected to hypo-osmotic stress (150 mOsm) for 5 min (B). The full data set is shown in table S6. (**C** to **E**) Analysis of the sizes and numbers of particles associated with anti-PABPC1 in the cytosol of control A10 cells and A10 cells treated with siRNA(PLCβ1) as measured with a 100x objective and analyzed with Image J software (see Materials and Methods). The indicated cells were analyzed under basal conditions (C), after being subjected to osmotic stress (150 mOsm) (D), and after treatment with 5 μM carbachol to stimulate $G\alpha_q$ (E). All measurements are an average of three independent experiments with 10 cells sampled per experiment. Error bars indicate SD. *P* values were determined by ANOVA.

Fig. 7. N&B analysis of eGFP-Ago2 aggregation in WKO-3M22 cells. (**A** to **C**) N&B analysis of brightness versus intensity for PC12 cells under the indicated conditions with the pixels of the colored boxes corresponding to specific regions in the cells (middle). Bottom: corresponding

fluorescence microscopy images. Red boxes correspond to monomeric eGFP-Ago2 as determined by free eGFP. Points outside this box and in the green and blue boxes correspond to higher-order species and where the percentage of aggregation is given in red. Data in (A) show control cells, data in (B) show cells subjected to hypo-osmotic stress (150 mOsm, 5 min), and data in (C) show cells subjected to carbachol stimulation (5 μM, 10 min). (**D** and **E**) Data in (D) show cells treated with siRNA(PLCβ1), whereas data in (D) and (E) show cells treated with siRNA(PLCβ1) and stimulated with osmotic stress (150 mOsm). Data are from three experiments with nine cells analyzed per experiment. (**F**) Plot of the size distribution of cytosolic RNAs of WKO-3M22 cells as measured by dynamic light-scattering for control conditions (black), osmotic conditions (150 mOsm 5 min, red), and stimulation of $G\alpha_q$ with carbachol (5 μM, 10 min, green).

Fig. 8. Relationship between particle formation and PLCβ1 abundance. (**A** and **B**) Analysis of the relationship between the number of PABPC1 particles and their average area in (A) PC12 cells and (B) A10 cells that were treated as indicated. (**C**) Analysis of the relationship between the number of PABPC1 particles determined in Fig. 4, A to C, and Fig. 6, C to E and the estimated concentration of total cytosolic PLCβ1 in PC12 and A10 cells where the intensity is compared to a calibration scale using Alexa488 and measuring in confocal volume in an FCS instrument (*26, 69*).

Fig. 9. Model of the multiple interactions of PLCβ1 in cells. Under basal conditions, PLCβ1 is distibuted both at the plasma membrane and in the cytosol where it may interact with stress granule–associated proteins. The activation of $G\alpha_q$ (through the stimulation of a GPCR by its

ligand) promotes the movement of PLCβ1 to the plasma membrane, thereby releasing the stress granule–associated proteins and promoting particle formation.

Fig. 1

A

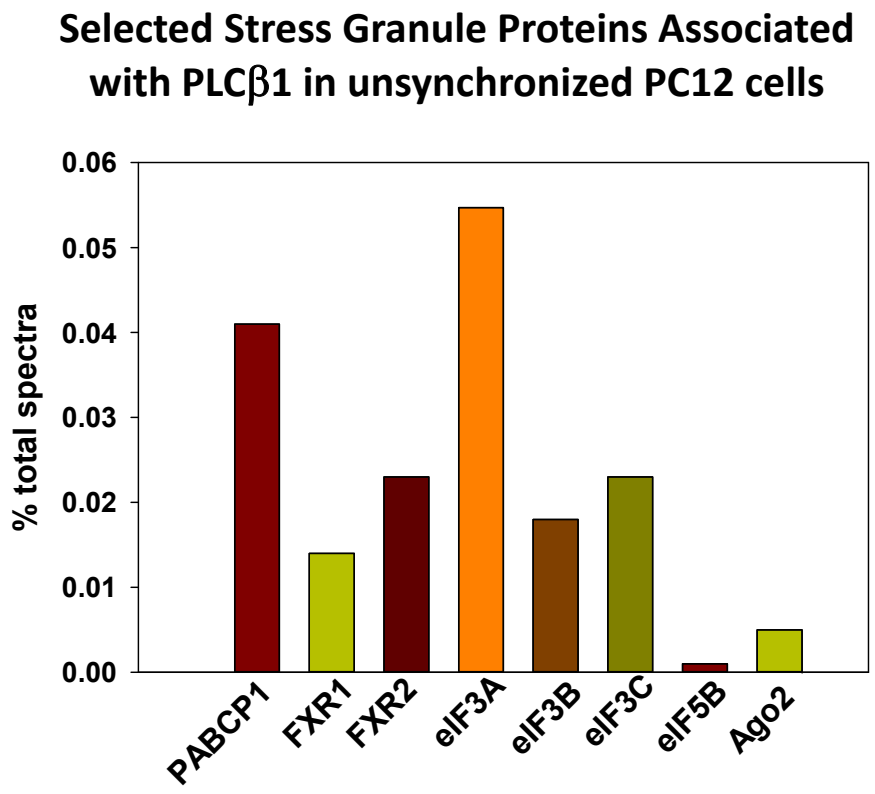

B

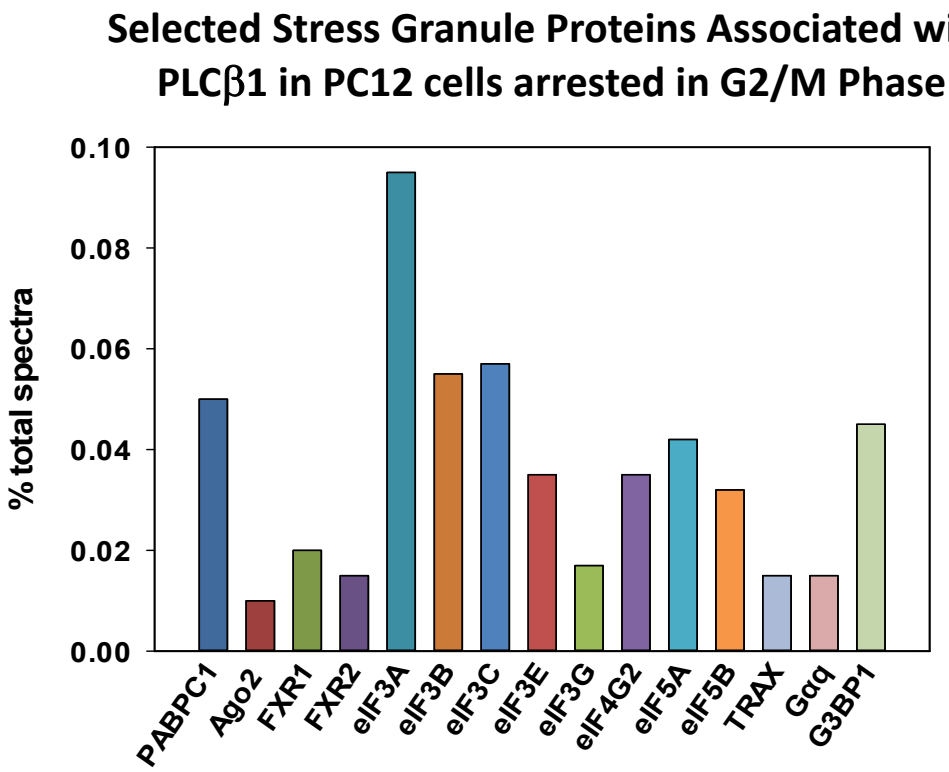

Fig. 2

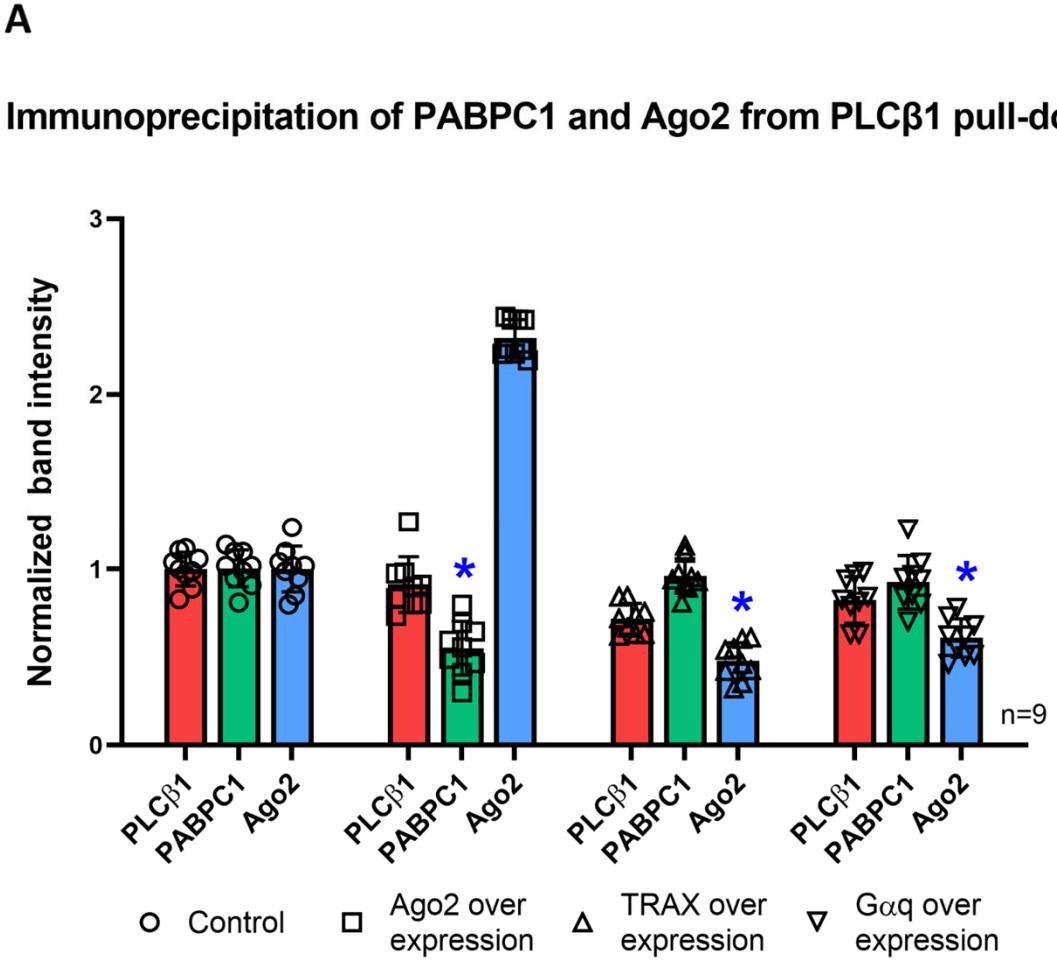

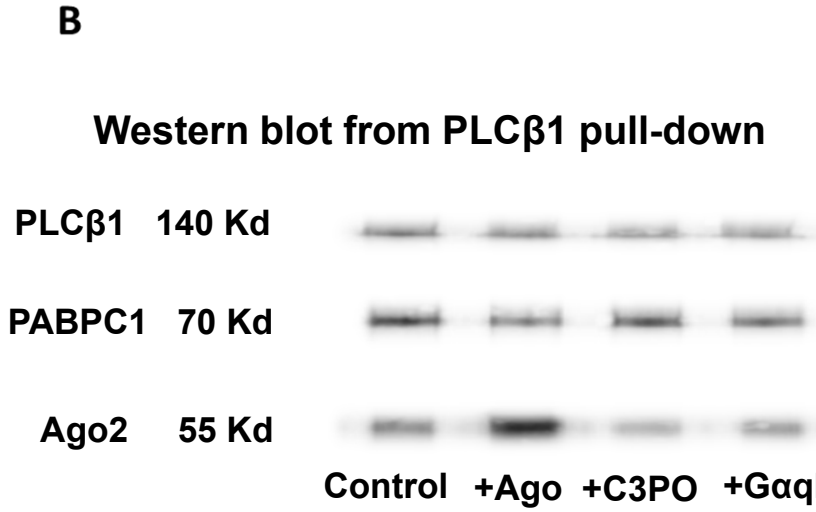

Fig. 2

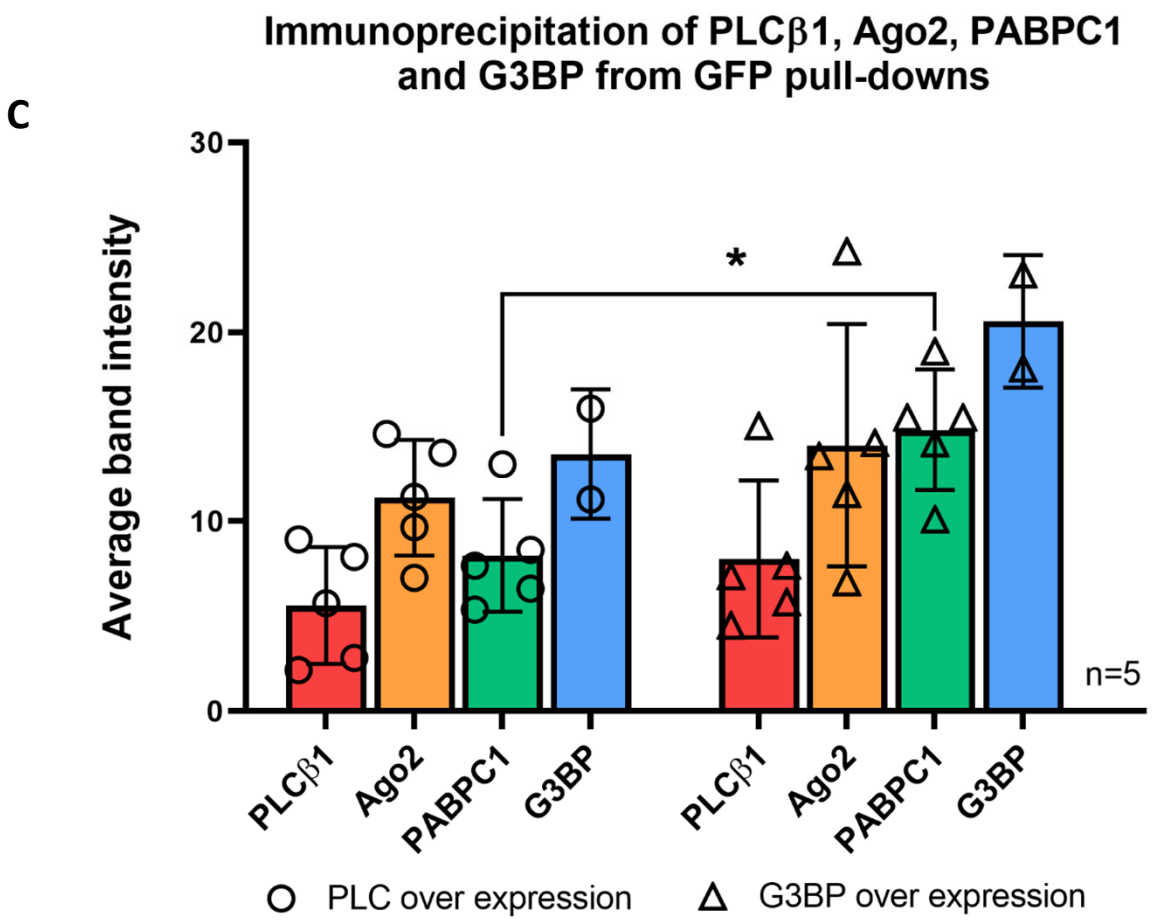

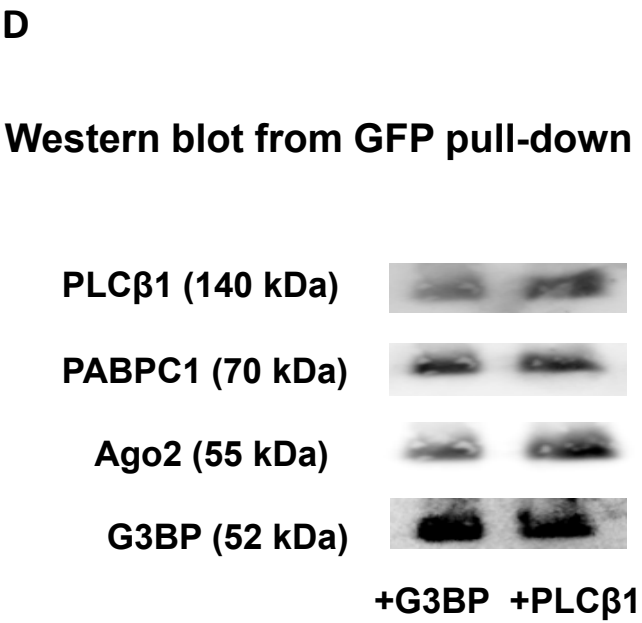

Fig. 3

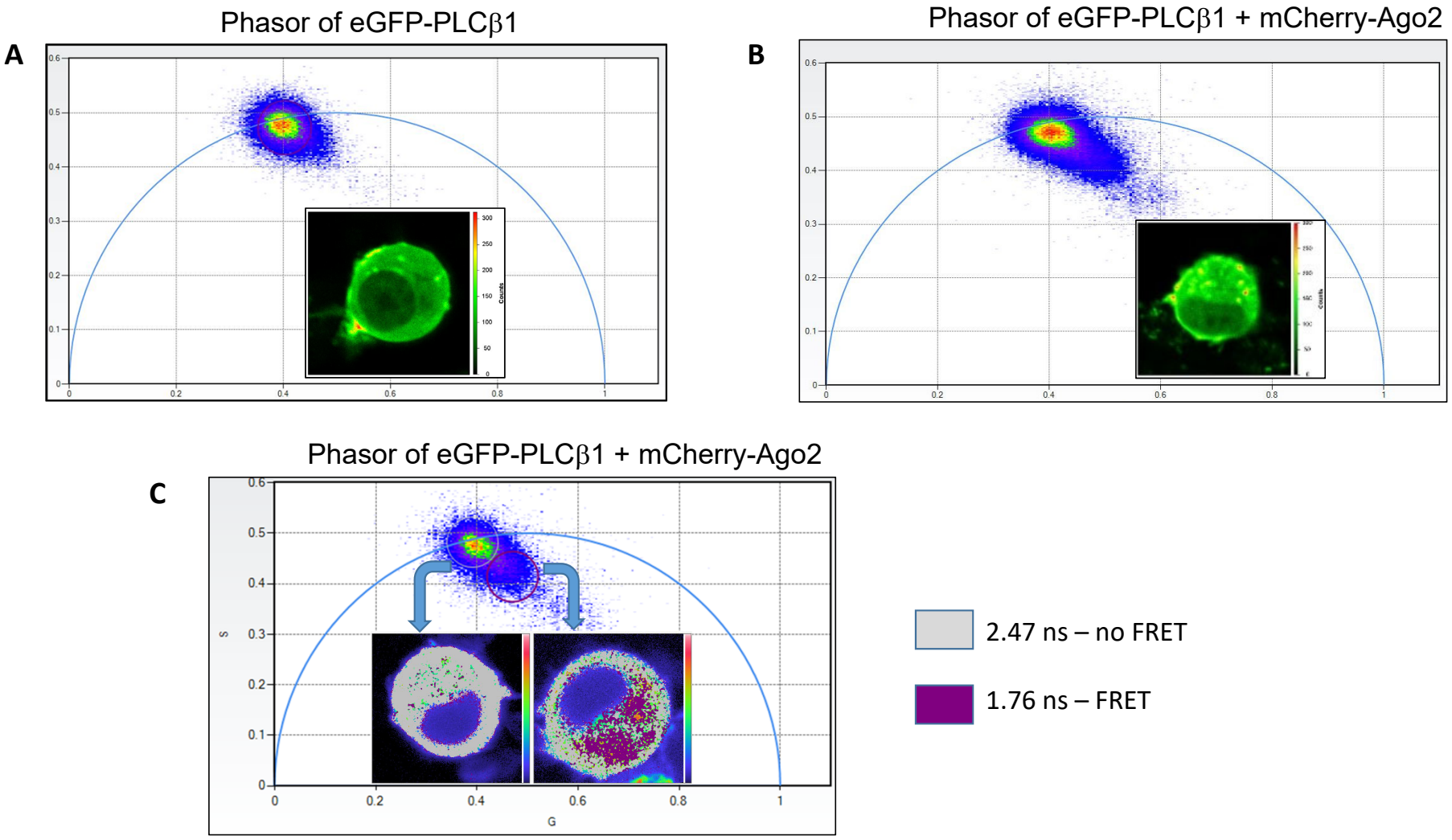

Fig. 4

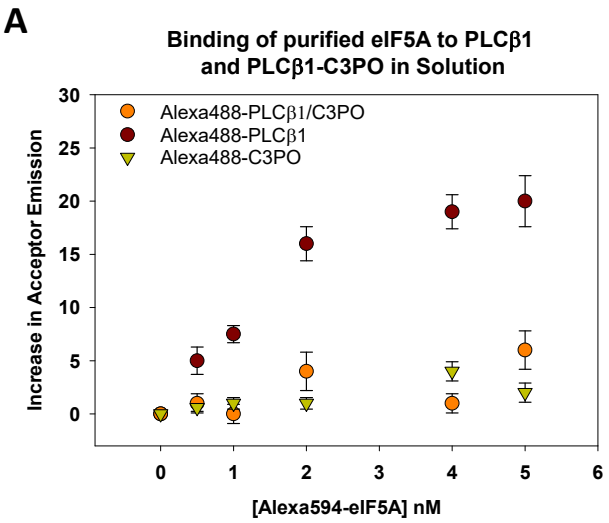

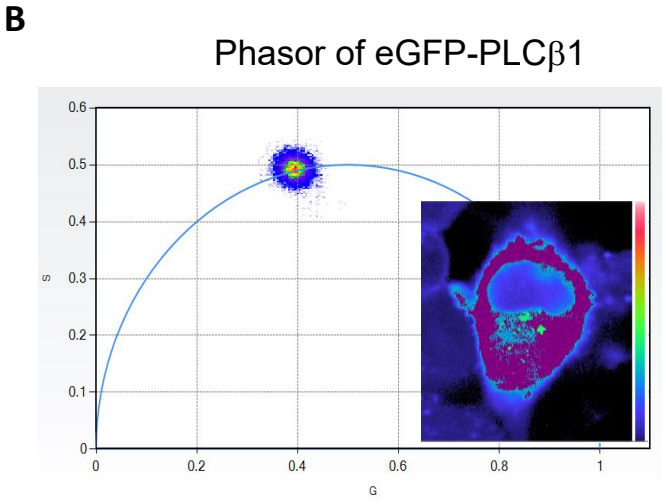

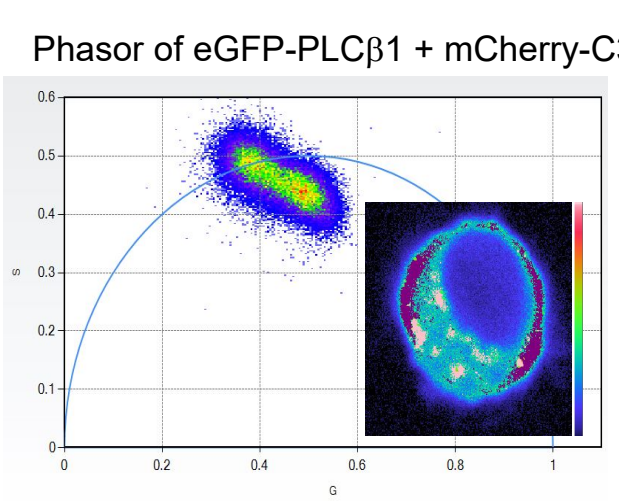

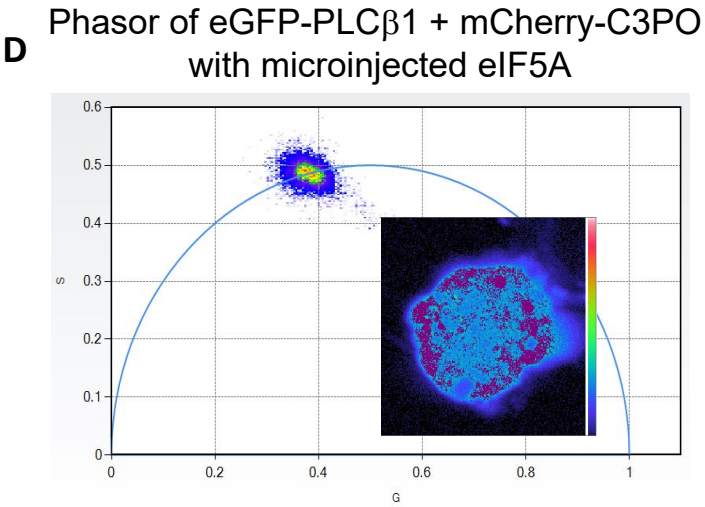

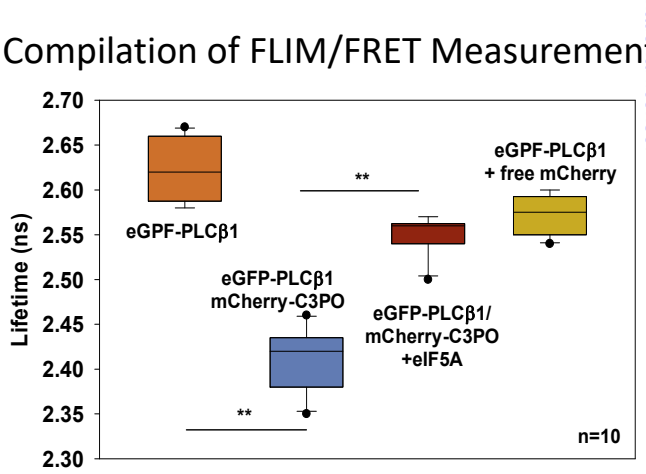

Fig. 5

A

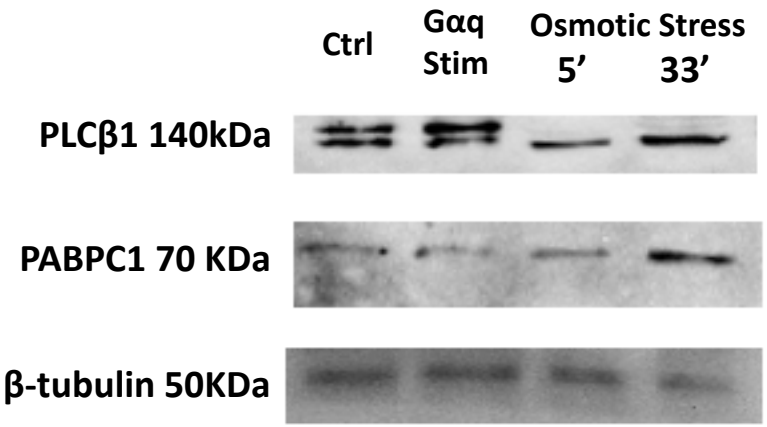

B

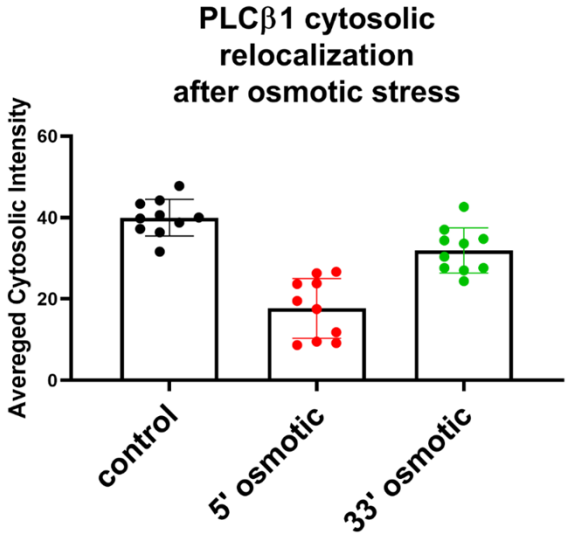

C

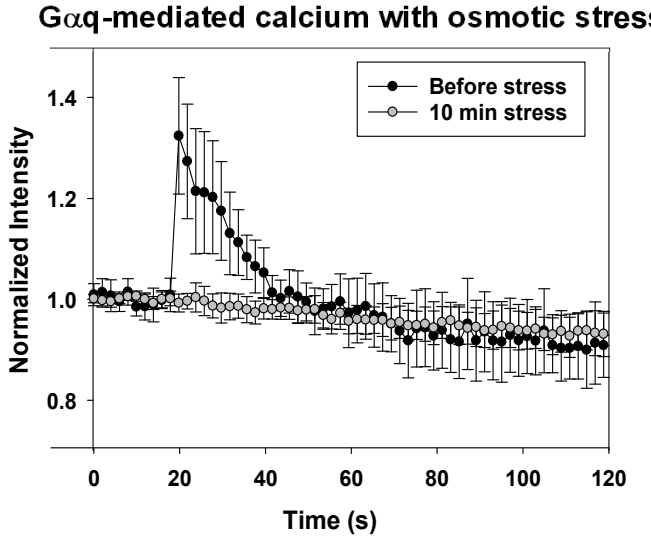

Fig.6

A

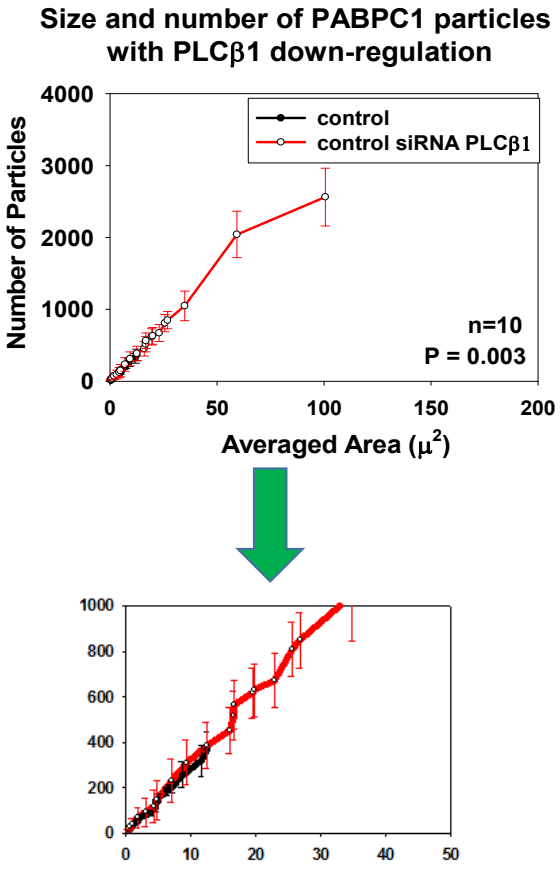

B

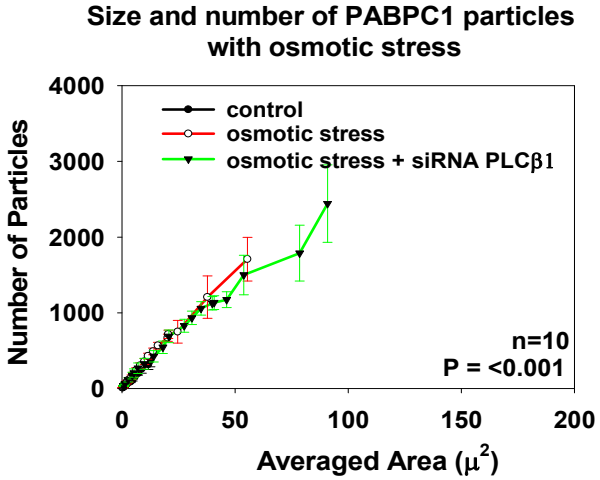

C

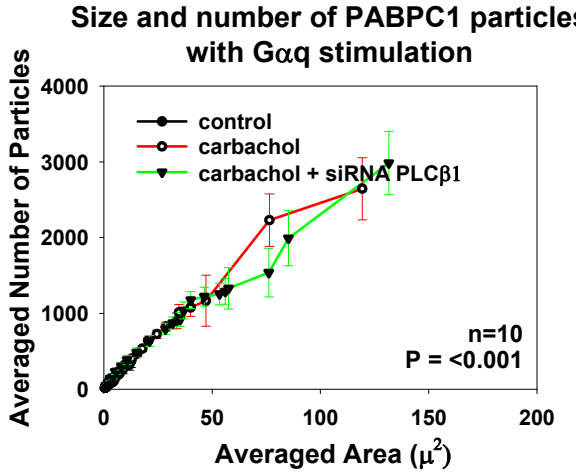

Fig. 7

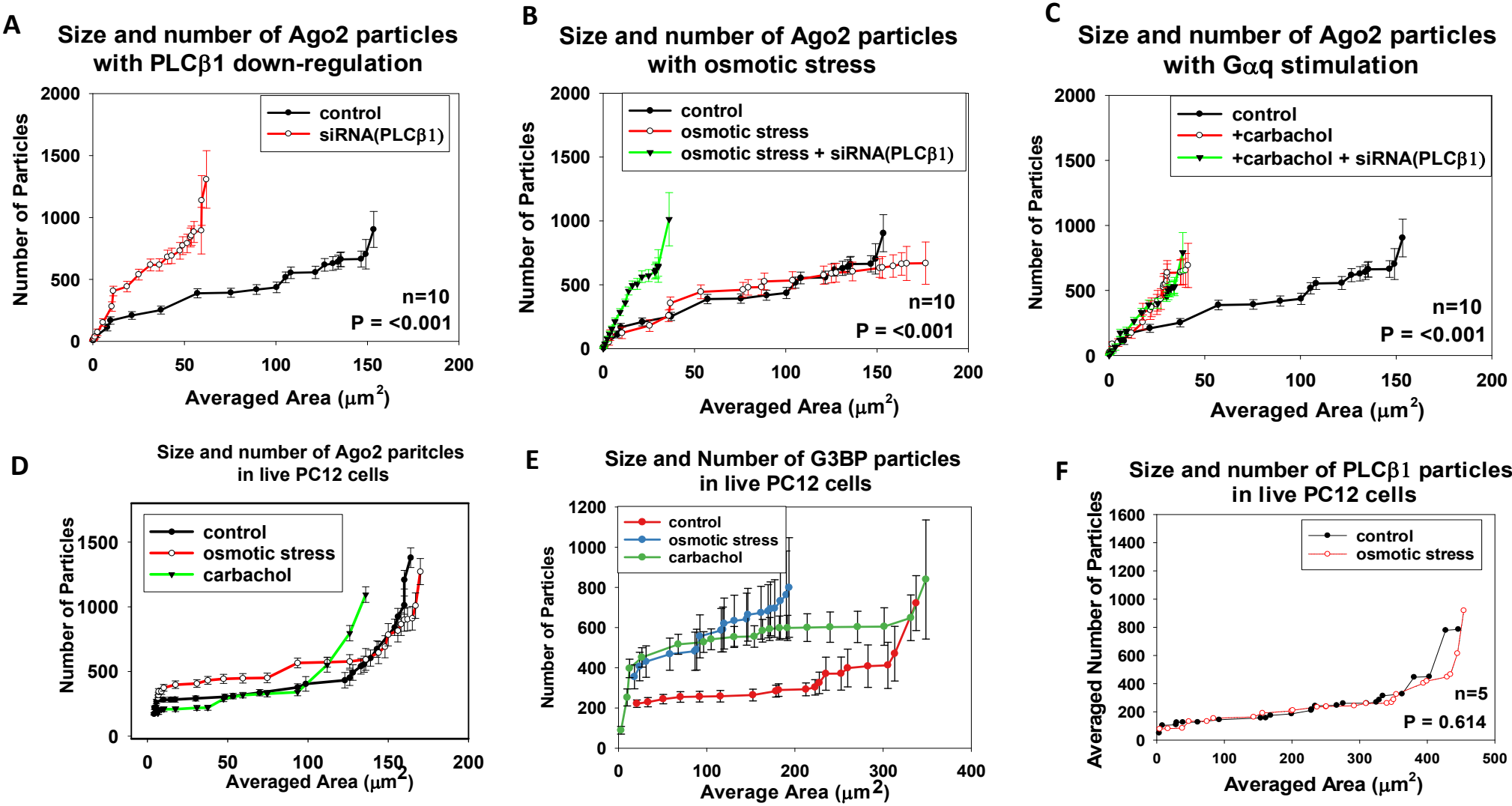

Fig 8

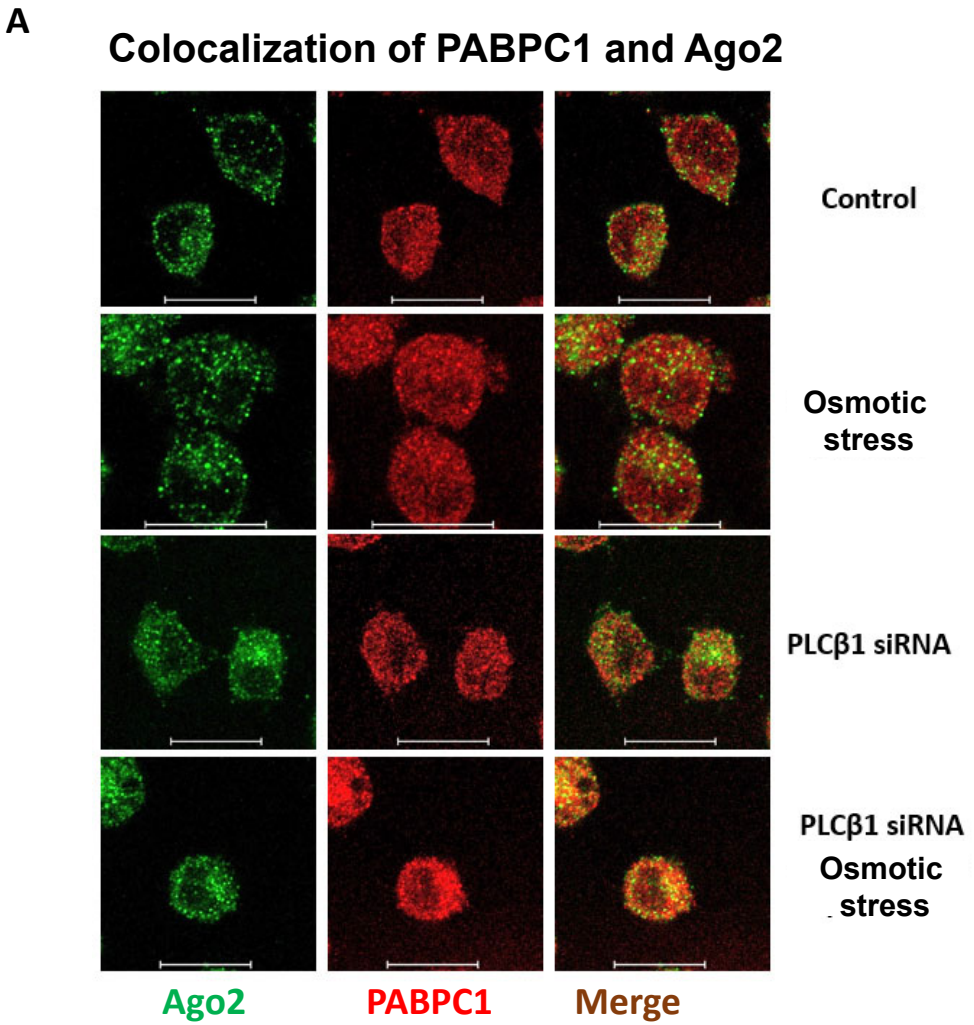

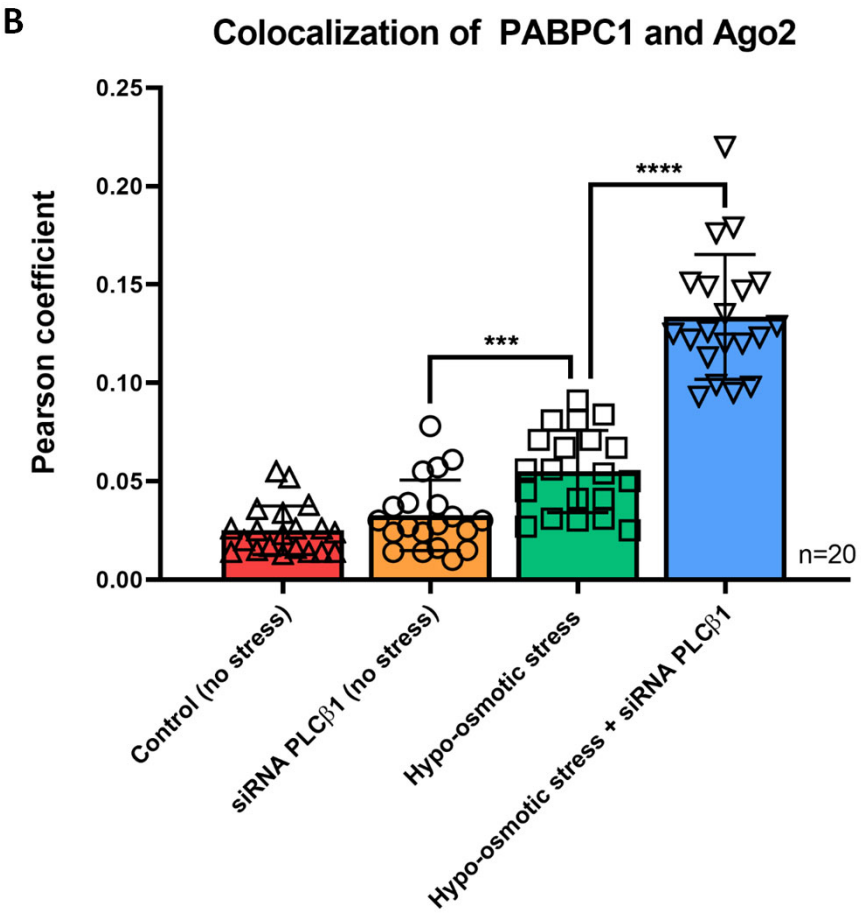

Fig. 9

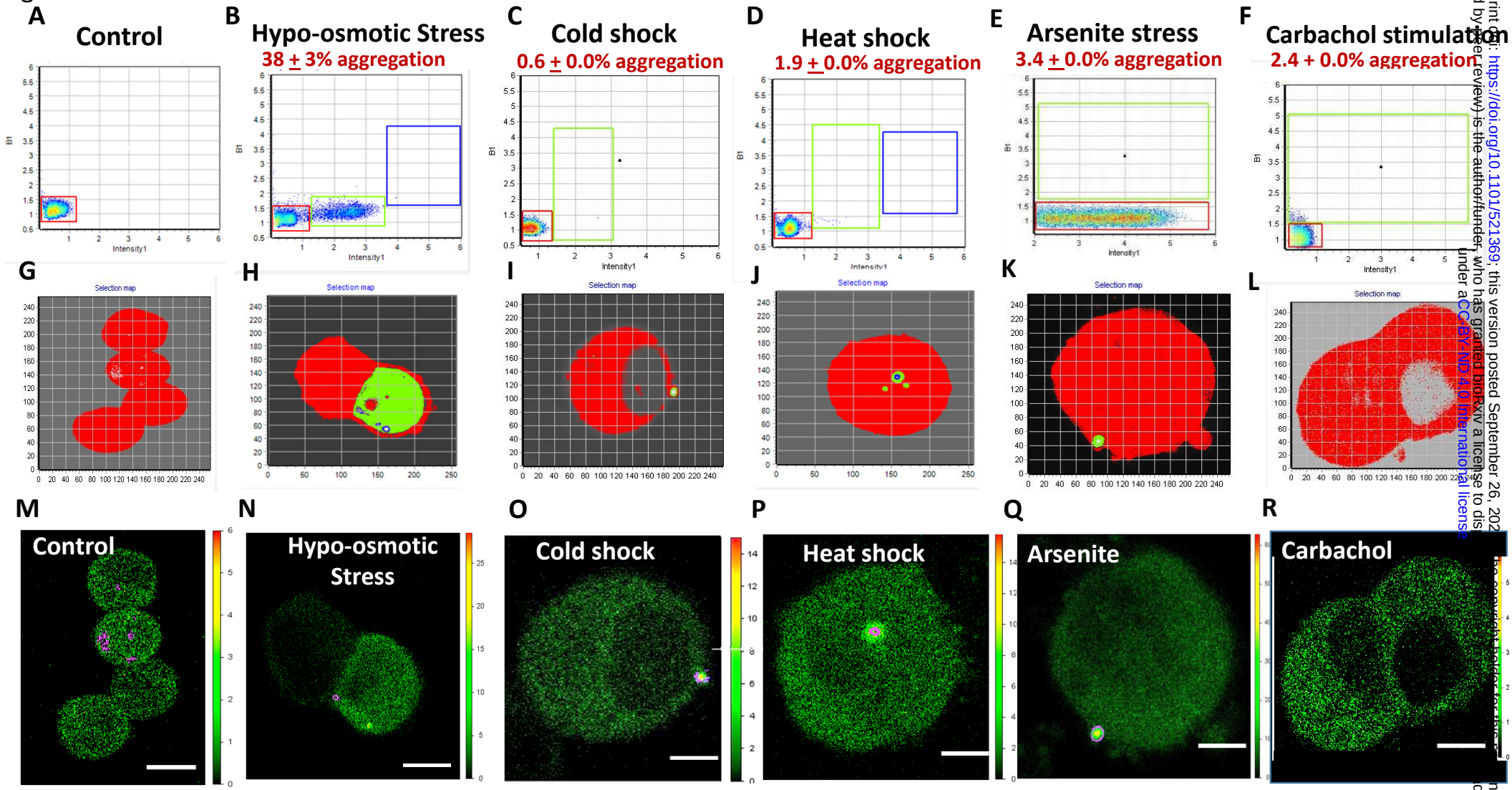

Fig. 10

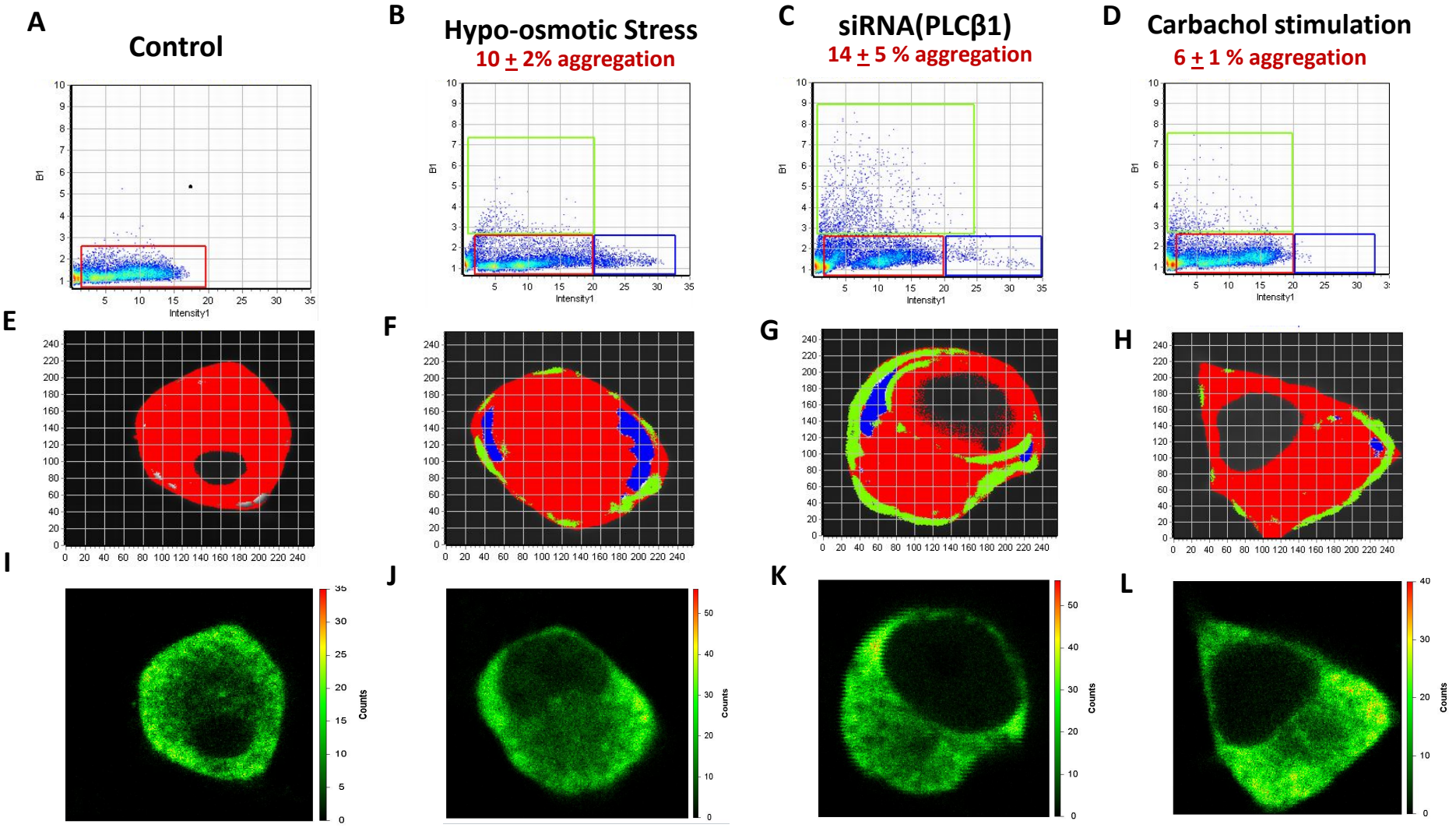

Fig. 11

Size distribution of cytosolic RNA from PC12 cells

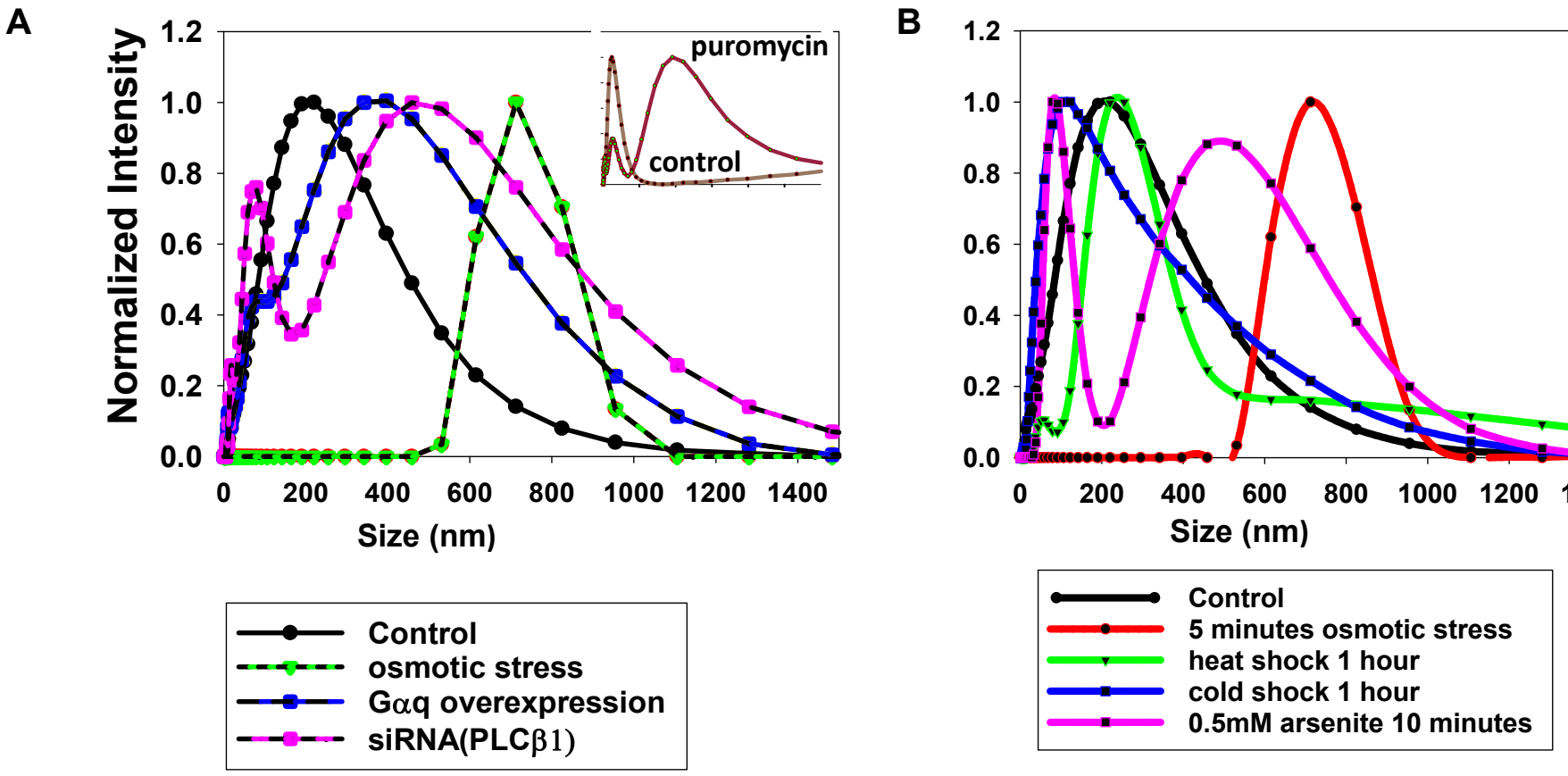

Fig. 12

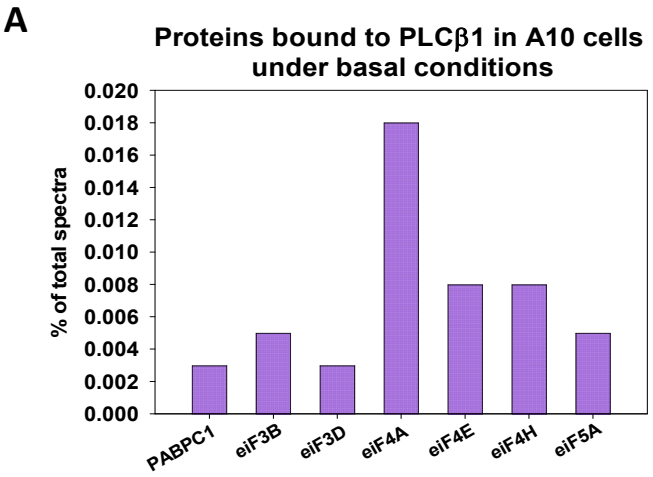

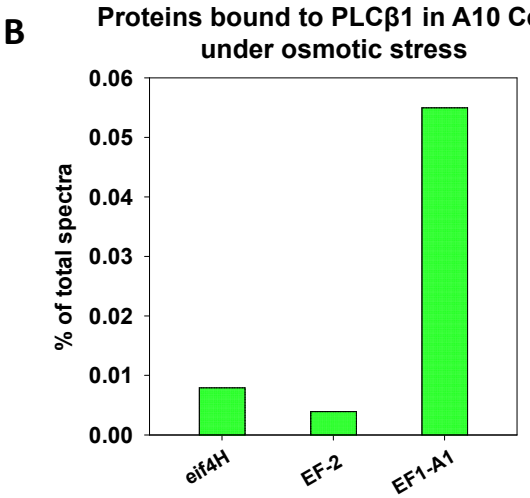

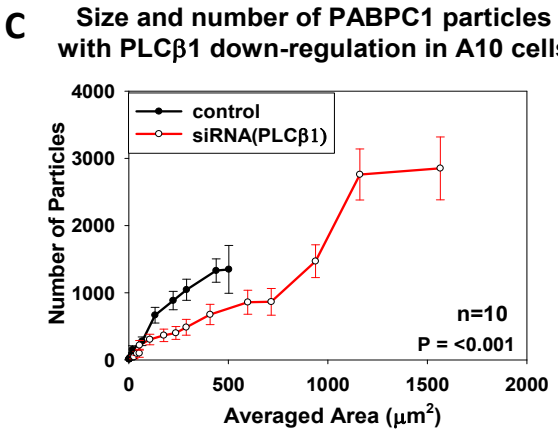

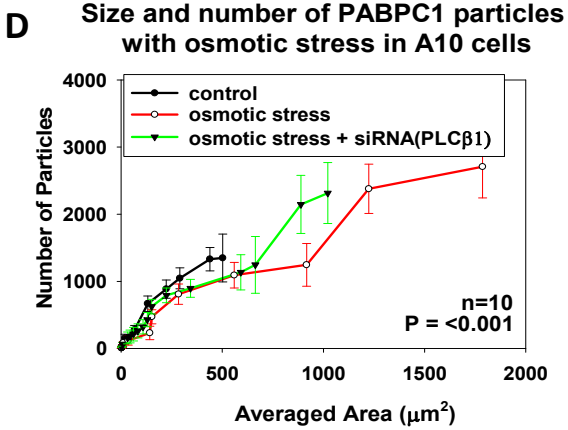

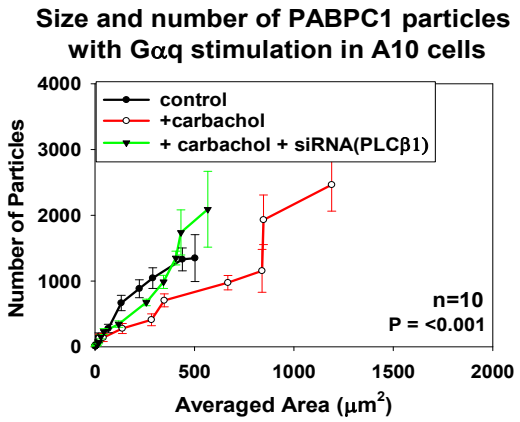

Fig. 13

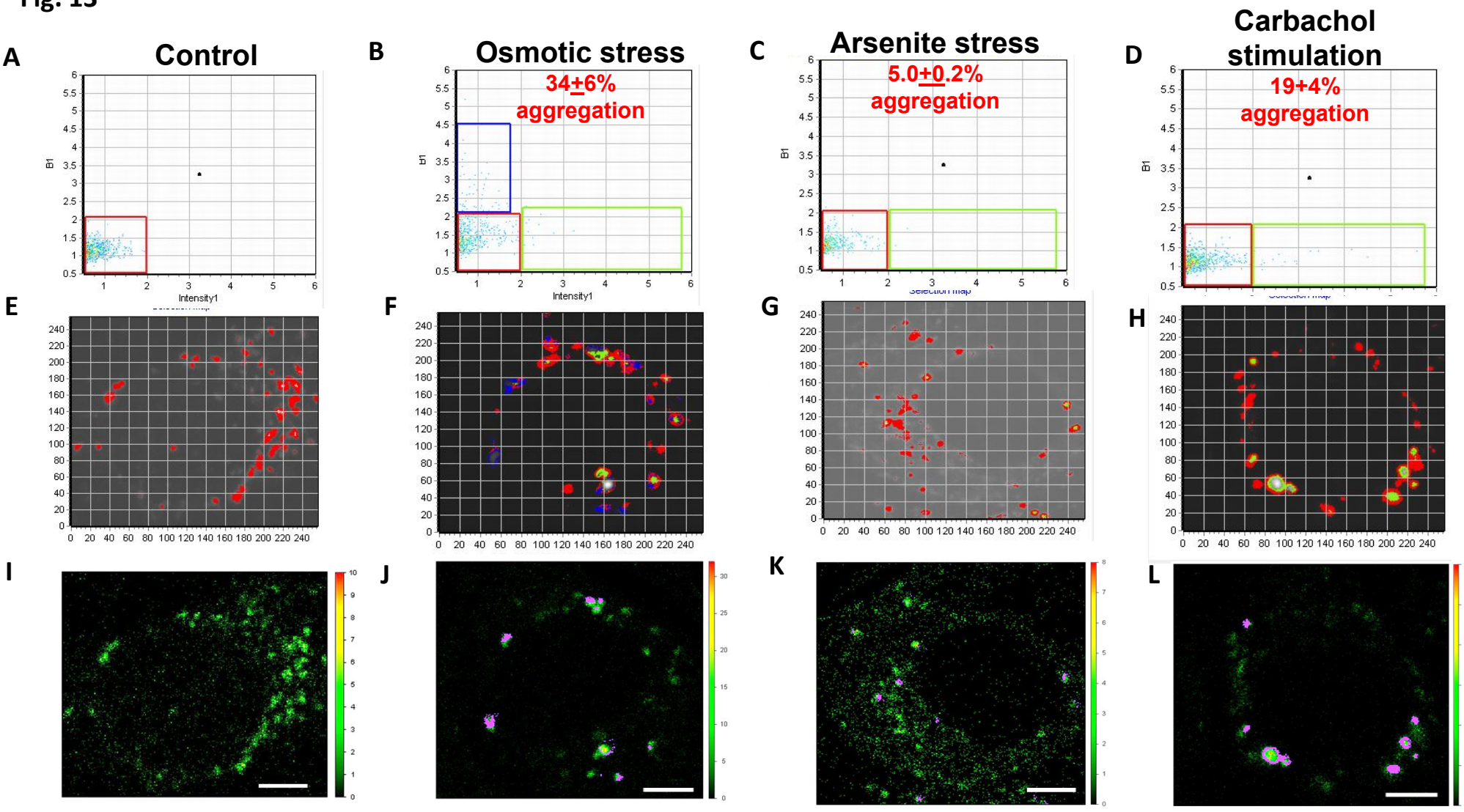

Fig. 13

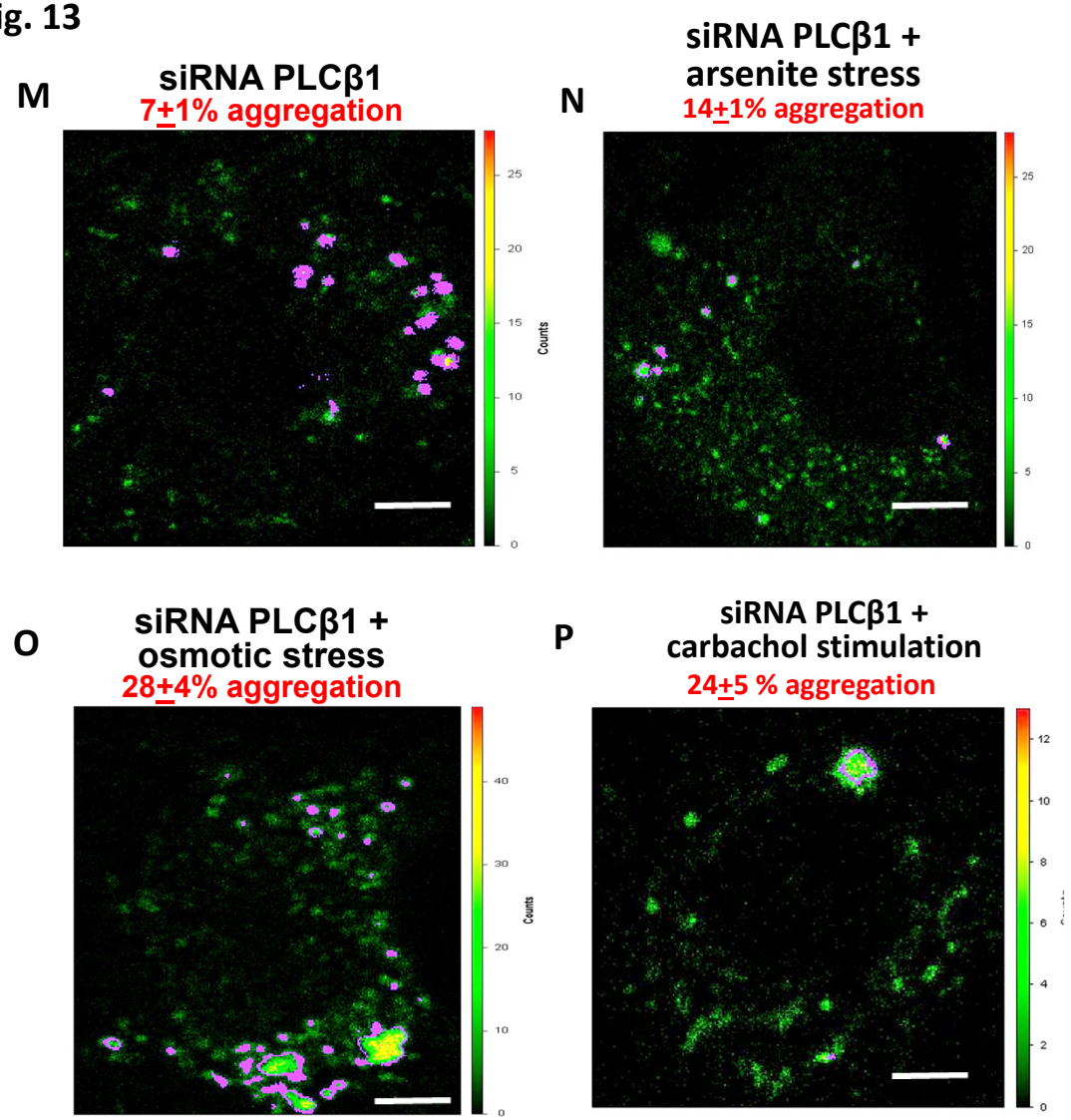

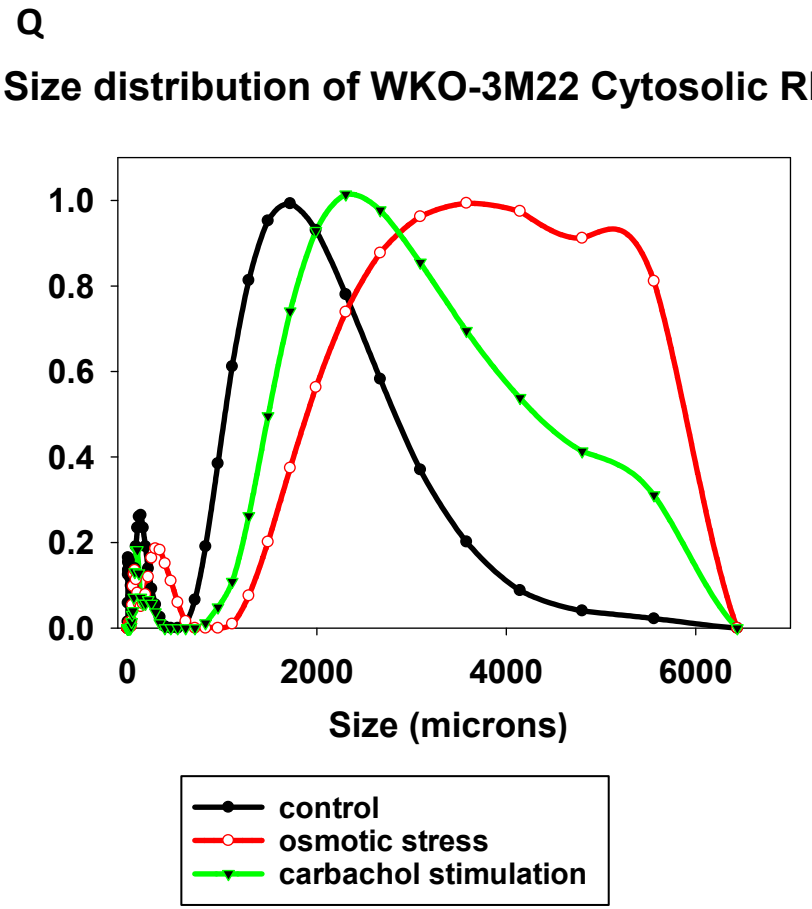

Fig. 14

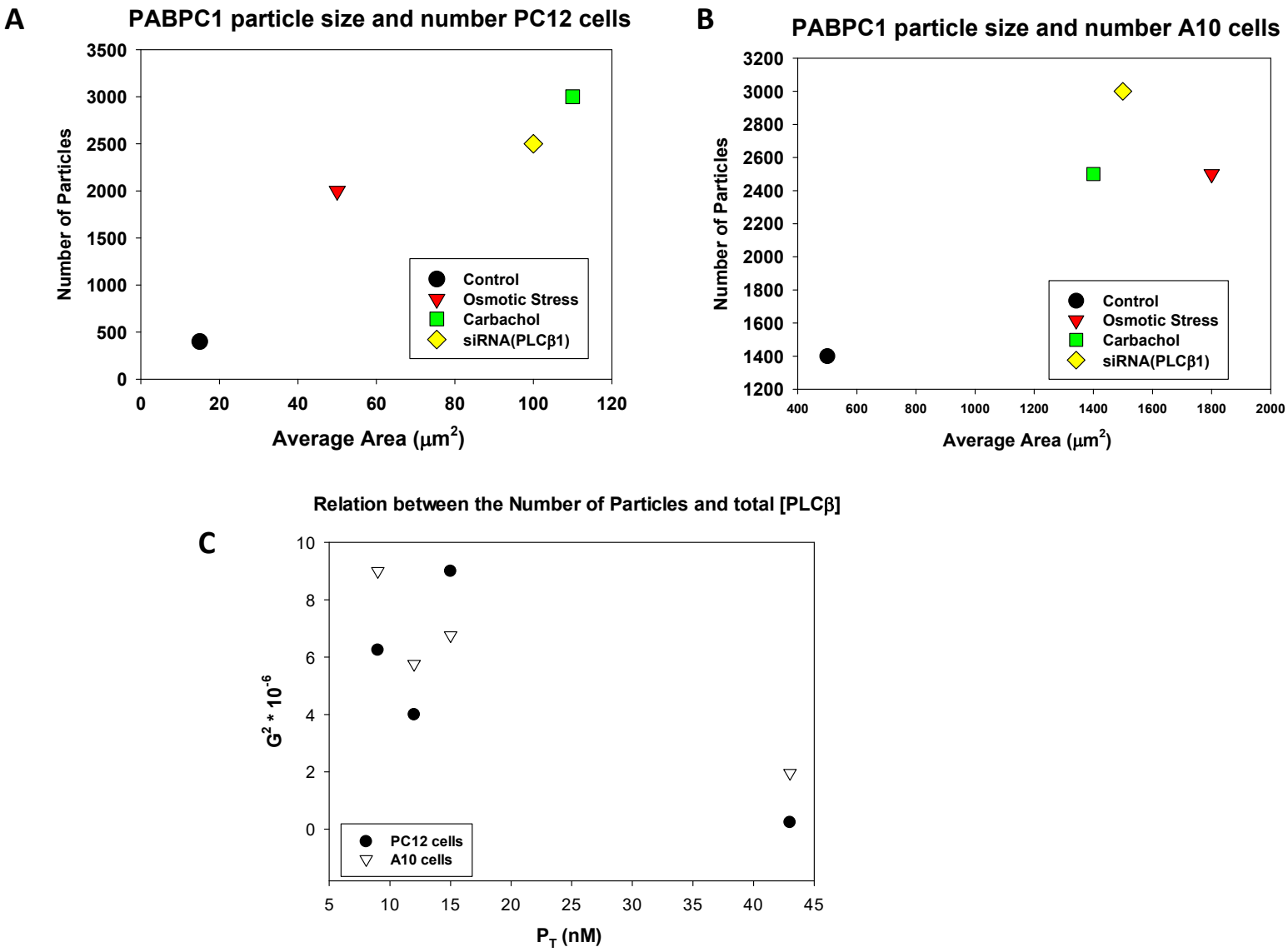

Fig. 15